

Review

Nanomaterials as a Sustainable Choice for Treating Wastewater: A Review

Wael Ben Mbarek ¹, Lluisa Escoda ¹, Joan Saurina ¹, Eloi Pineda ², Fahad M. Alminderej ³, Mohamed Khitouni ³ and Joan-Josep Suñol ^{1,*}

¹ Department of Physics, Campus Montilivi s/n, University of Girona, 17003 Girona, Spain

² Department of Physics, Institute of Energy Technologies, Universitat Politècnica de Catalunya, 08019 Barcelona, Spain

³ Department of Chemistry, College of Science, Qassim University, Buraidah 51452, Saudi Arabia

* Correspondence: joanjosep.sunyol@udg.edu

Abstract: The removal of dyes from textile effluents utilizing advanced wastewater treatment methods with high efficiency and low cost has received substantial attention due to the rise in pollutants in water. The purpose of this work is to give a comprehensive analysis of the different treatments for removing chemical dyes from textile effluents. The capability and potential of conventional treatments for the degradation of dyeing compounds in aqueous media, as well as the influence of multiple parameters, such as the pH solution, initial dye concentration, and adsorbent dose, are presented in this study. This study is an overview of the scientific research literature on this topic, including nanoreductive and nanophotocatalyst processes, as well as nanoadsorbents and nanomembranes. For the purpose of treating sewage, the special properties of nanoparticles are currently being carefully researched. The ability of nanomaterials to remove organic matter, fungus, and viruses from wastewater is another benefit. Nanomaterials are employed in advanced oxidation techniques to clean wastewater. Additionally, because of their small dimensions, nanoparticles have a wide effective area of contact. Due to this, nanoparticles' adsorption and reactivity are powerful. The improvement of nanomaterial technology will be beneficial for the treatment of wastewater. This report also offers a thorough review of the distinctive properties of nanomaterials used in wastewater treatment, as well as their appropriate application and future possibilities. Since only a few types of nanomaterials have been produced, it is also important to focus on their technological feasibility in addition to their economic feasibility. According to this study, nanoparticles (NPs) have a significant adsorption area, efficient chemical reactions, and electrical conductivity that help treat wastewater effectively.

Keywords: nanocatalysts; nanomembranes; nanoadsorbents; wastewater treatment; nanomaterial challenges



Citation: Mbarek, W.B.; Escoda, L.; Saurina, J.; Pineda, E.; Alminderej, F.M.; Khitouni, M.; Suñol, J.-J. Nanomaterials as a Sustainable Choice for Treating Wastewater: A Review. *Materials* **2022**, *15*, 8576. <https://doi.org/10.3390/ma15238576>

Academic Editors: Evgeny Parfenov and Elena Korznikova

Received: 24 October 2022

Accepted: 28 November 2022

Published: 1 December 2022

Publisher's Note: MDPI stays neutral with regard to jurisdictional claims in published maps and institutional affiliations.



Copyright: © 2022 by the authors. Licensee MDPI, Basel, Switzerland. This article is an open access article distributed under the terms and conditions of the Creative Commons Attribution (CC BY) license (<https://creativecommons.org/licenses/by/4.0/>).

1. Introduction

Dyed effluents are of great environmental concern. Textile industries consume a large amount of water and produce a remarkable amount of wastewater containing pigments, dyes, and non-expendable components. Dyes give off their color by staining or being absorbed after their dissolution in specific solutions. Various atomic groups, known as chromophores, determine whether an organic source seems to be a dye or not. The azo group, thio group, nitroso group, carbonyl group, nitro group, and azoxy group are examples of chromophores. Auxochromes are different groups of atoms that link to dye molecules, contribute or receive electrons, improve color, and boost solubility. Auxochrome groups consist of substituted amino, hydroxyl, sulfonic, and amino groups. Dyes are classified depending on how well they color. There are various dyes used, and even more textiles and materials now contain colorants during production. Depending on the chemical

characteristics of the dye and the physical characteristics of the material to be dyed, or the dyeing properties, certain dyes are employed for specific materials. Basic or cationic, acid and premetallized, chrome and mordant, direct, sulfur, dispersion, vat, azoic, and reactive dyes are the different categories of dyeing characteristics.

The generation of wastewater that is highly polluted and contains dyes is a very serious problem for sewage treatment stations. In addition, there are some highly toxic materials and textile waste products that are responsible for reducing the ability of self-decomposition of pollutants in wastewater [1]. Physical, chemical, and biological approaches are three that are frequently used to address the degradation of residual azo dyes in wastewater. Examples of physical and chemical treatments include adsorption, flocculation, electro-coagulation, precipitation, ozonation, and irradiation. However, these procedures may be not enough to eradicate dyes from wastewater. For example, the biological method is not suitable for eliminating color from dyes because most of them are inorganic and toxic to the microorganisms used in the process. However, physical techniques, such as membrane filtering, ion exchange, and adsorption, have key limitations: they work best when the volume of wastewater is modest and can be further broken down into a few tiny components that are challenging to digest. During the molecular process of adsorption, forces of attraction bind a solute (adsorbate) to a solid surface (adsorbent). The coagulation–flocculation procedure is widely used as a pretreatment stage to improve the effectiveness of subsequent processes, such as sedimentation and filtration, in a water treatment system. In the coagulation process, the coagulant is primarily responsible for destabilizing the colloidal particles. The flocculation process, which increases the solution's unstable particle size into larger flocs, comes next. This technique enables the removal of suspended solids and colloidal particles from the solution. Large amounts of organic contaminants can be effectively removed using the coagulation and flocculation process [2]. In addition, researchers have been very interested in plasma technology for a variety of environmental applications [3]. Pesticides in wastewater can be detoxified and degraded using cold (non-thermal) plasma technology, which does not create any secondary pollutants in the process [4]. Due to the creation of UV radiation, shock waves, and highly reactive species that oxidize and mineralize the contaminants into CO₂, H₂O, and simpler inorganics, cold plasma is also a well-known technique for cleaning water.

In order to change the phases, physical treatments, such as filtration, can be utilized to eliminate the contaminants. However, this modification leads to the release of a significant amount of sludge, which is hazardous to the environment and difficult to dispose of [5,6]. In addition, most dyes exacerbate the environmental problem due to the formation of undesirable decomposition products [7]. The degradation of dyes from textile waste can be very difficult due to their complex structure [8].

To the best of our knowledge, despite the wide range of studies in this field, there are not many review articles that have discussed the use of nanomaterials in the degradation of organic dyes in wastewater. Throughout this review paper, we have attempted to investigate the synergistic impact of using nanomaterials in the degradation of organic pollutants as well as discuss their efficacy in the reduction of contaminants and the reuse of wastewater in industrial cycles. The most suitable technology to effectively and economically eliminate contaminants is nanotechnology, which is seen as an emerging discipline that offers an alternative [9]. The nanomaterials range in size from a few nanometers to less than 100 nm [10]. Occasionally, specimens with nanostructures are regarded as nanomaterials. Around the world, there are several environmental problems that nanomaterials can potentially solve. Nanomaterials come in a variety of forms, including nanowires, nanotubes, films, particles, colloids, and quantum dots [11]. Nanophotocatalysts, nanoreductives, nanomembranes, and nanosorbents are the four main types of nanomaterial that can play a crucial part in the wastewater treatment process (Figure 1). The distinctive attributes of nanomaterials, such as their high surface area, large pores, high reactivity, strong mechanical properties, ease of dispersion, and hydrophobic/hydrophilic characteristics, have been demonstrated by researchers to be suitable candidates for wastewater technology [12,13]. These approaches

have been used in several studies to remove dangerous microbes, organic and inorganic contaminants, and poisonous heavy metal ions [14–16]. Therefore, the purpose of the current review is to outline the four types of nanomaterials' potential contributions to the removal of these organic contaminants from wastewater. Additionally, this review summarizes the potential drawbacks of the techniques using nanomaterials as enhancements and highlights the difficulties that must be addressed in order to produce sustainable technologies in great detail.

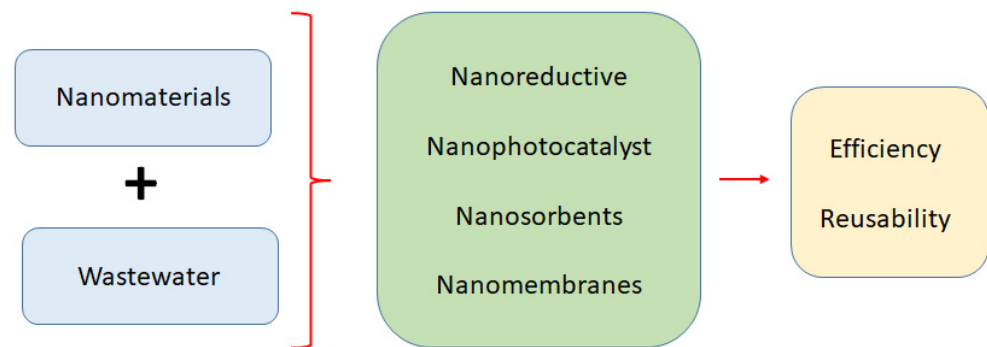


Figure 1. Nanomaterials and processes in the wastewater treatment.

2. Nanoreductive Processes

Nanomaterials can greatly improve water treatment and pollution control due to their exceptional adsorption capabilities, exceptional chemical characteristics, excellent mechanical properties, affordability, and power efficiency [17]. These compounds function as adsorbents and are distinguished by their clearly defined and controllable structures, as well as their suitable porosity and size [18]. NPs are used in wastewater to filter out other 1–100 nm particles, including viruses and organic material [19]. Unlike their larger cousins, which lack the same outstanding properties due to their small size and lack of structural and chemical features, NPs have impressive properties [20]. NPs frequently have a few hundred atoms in them [21]. The suitability of NPs for a given application is determined by a number of qualities, including physical, chemical, electrical, magnetic, and optical qualities, among others [22]. Other important chemical and physical properties exist in addition to the number of dimensions, form, chemistry, composition, surface size and arrangement, morphology, and hardness. NPs exhibit electrical properties based on their chemical composition in addition to their surface area, size, and chemical composition [9].

For industrial-level dye removal, reductive degradation is a rapid and inexpensive procedure that is simple to use. The following particles, including nanoparticles, have been used to date to remove azo dyes. A schematic representation of the Ca–Al system's role in Mbarek et al.'s hypothesized degradation mechanism for RB5 is shown in Figure 2 [23]. Owing to its tiny particle size, nanoscale zerovalent iron (nZVI) quickly agglomerates to form necklace-like arrangements, according to experimental research [24,25]. The high reactivity of nZVI systems can only be attained when the wastewater is in an acidic condition (pH below 5.0), according to Xiong et al. [26].

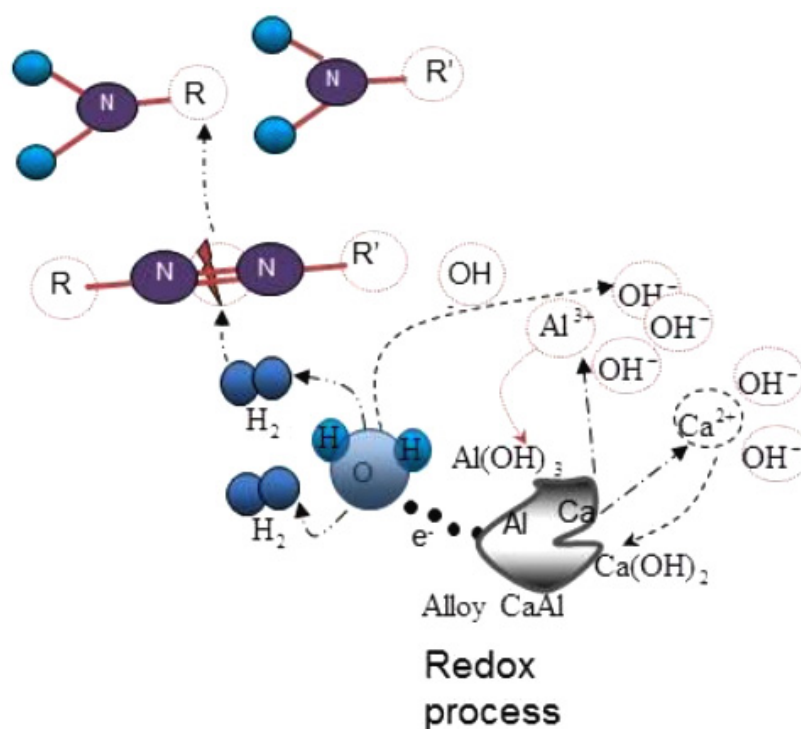


Figure 2. Schema of the proposed degradation mechanism of RB5 using $\text{Ca}_{65}\text{Al}_{35}$ compound. Reprinted/adapted with permission from Ref. [23]. 2017, Elsevier.

A laboratory-scale slurry reactor system was used by Bigg et al. to explore the kinetics of reductive degradation of two distinct azo dyes in aqueous solution. The reaction kinetics for the reductive degradation of both dyes exhibited pseudo first-order behavior. At mixing speeds of 2000 revolutions per minute, the average rate constant for the reactions was 0.735 min^{-1} and 0.694 min^{-1} for acid orange II and acid blue 113, respectively. The apparent rate constant (k) was reduced with the initial dissolved oxygen content and pH, but the mixing speed and iron content both led to increases in this value. Both acid orange II and acid blue 113 exhibited a linear increase with iron concentration, with correlation coefficients of $3 \times 10^{-5} \text{ mg L}^{-1}$. For both dyes, the rate constant rose linearly with the inverse square root of the mixing speed, directly proportional to the rise in reaction rate as the thickness of the boundary layer decreased. Acid orange II's half-lifetime correlated closely with the values given in the literature. A qualitative description of the impact of mass transfer on the reaction rate is provided by the mass transfer theory, and a quantitative one is provided by the empirical Sherwood number and the thickness of the stationary boundary layer that attaches to the iron particle. In terms of the initial dissolved oxygen concentration in the aqueous phase, the impact of surface passivation is quantitatively proved [27].

Mixing nZVI with a noble metal is a well-documented method used to increase the material's chemical reactivity (Pd, Pt, Ag, Ni, etc.). A lot of experimental works using bimetallic nZVI for pollutant remediation have been conducted recently, including Fe/Pd [28–32], Fe/Pt [32], Fe/Ag [33], and Fe/Ni [29,34–37]. Fe^0 is thought to act as an anode in these electrochemical couples, becoming sacrificially oxidized to galvanically preserve the noble metal. Particle performance in experiments has varied, with Fe–Pd generally outperforming the other combinations. It is thought that the noble metal directly transfers electrons to the sorbed pollutants at the bimetallic nZVI surface, or that hydrogen produced by the oxidation of Fe^0 reacts with the contaminants. Most likely, there is hydrogen in the form of a dissolved gas, some of which is adsorbed to the surface of the particles, and an undetermined portion that may be present as an active metal hydride that underwent diatomic dissociation and reacted with the exposed noble metal [29].

High entropy alloys (HEAs) are recently developed materials in the field of metallic materials research [38]. Many desirable characteristics of HEAs have been discovered in recent scientific and technological research, including their mechanical properties [39–41], strong temper-softening resistance [39,40], good thermal stability [42], and great corrosion resistance [43,44]. Due to their fast decolorization, environmental protection, low cost, and low efficiency [45,46], high entropy alloys have the potential to be used in wastewater treatment. At this time, it has been reported that zerovalent iron [47,48], Mn–Al binary alloys [49], and Al-based metallic glass alloys [50] show considerable decolorization properties for azo dyes. Additionally, it has been shown that a number of elements, including Fe, Cr, and Mn, which all have BCC crystal structures, and Al, Ti, Zn, and Co, exhibit significant activity. Even though aluminum has an FCC crystal structure, its high activity allows it to operate as a component of an alloy with a high entropy, which leads to the creation of the BCC phase [51].

Wu et al. reported on the decolorization of the azo dye direct blue 6 (DB6) using high entropy alloys (HEAs): the ball-milled (BM) AlCrFeMn and AlCrFeMnM (M = Mg, Ti, Ni). These alloys have significant azo dye decolorization properties and are in line with pseudo first-order exponential decay kinetics. AlCrFeMn had a superior performance to BM MgZn-based glassy powders, decolorizing DB6 three times more rapidly. AlCrFeMnMg and AlCrFeMnTi had a reaction activity that was approximately 2 and 1.2 times higher than AlCrFeMn, respectively. In the decolorization of the azo dye DB6, BM AlCrFeMn and AlCrFeMnMg operated excellently, and their reaction activities were three and seven times faster than BM MgZn-based metallic glass, respectively. It is more difficult to decolorize materials with increasing dye concentrations. In comparison to neutral solutions, AlCrFeMnMg reacted around 37.5 and 16.6 times more rapidly in alkaline and acidic azo dye solutions, respectively. In the application of azo dye decolorization and degradation, HEAs have good research value and do not contribute to secondary pollution [39].

According to Sha et al., hollow Co nanoparticles were produced using the galvanic replacement process, showed rapid catalytic activity during the degradation of methyl orange, and easily converted methyl orange into amine compounds. The azo dye degradation efficiency reached up to 99% in 4 min, and the degradation constant rate was up to 2.444 min^{-1} , with an initial methyl orange concentration of 100 mg/L (pH = 2.5) and 0.5 g/L of Co nanoparticles. The pH was a major factor in the dye degradation rates, and acidic environments were ideal. The rate at which methyl orange degrades is increased by the hollow nanoparticles' significantly higher surface area for high concentration organic chemical adsorption and surface reactions compared to solid nanoparticles [52].

According to works by Mbarek et al. and Abolighasembadi et al. [49,53,54], mechanically alloyed powders of manganese–aluminum (Mn85Al15) and calcium–aluminum (Ca65Al35) [23] demonstrated good efficiency and rapid response rates as decolorization agents for azo dye aqueous solutions. First, the effectiveness of powders produced using various manufacturing processes was compared in order to study the impact of the crystalline phase and microstructure. Second, the effectiveness of decolorization was examined using several dyes and actual textile wastewater samples. Although significant adsorption on the metallic surface was noted for several colorants, an analysis of the treated water and particle samples revealed that the predominant reaction mechanism included the degradation of azo dye molecules. Finally, it was determined whether the particles could be reused and whether the treatments had successfully reduced the toxicity. Manganese–aluminum powders have a variety of advantages over other highly efficient decolorizing metallic compounds, including easy production and application processes, high efficacy, and the use of environmentally favorable metallic elements. Additionally, Mbarek et al. investigated how adding Fe and Co affected the ability of mechanically alloyed Mn–Al powders to degrade azo dyes. The Mn–Al–Fe powder had remarkable degrading efficiency, and it was demonstrated that the reaction's kinetics were more rapid than those of Mn–Al-based alloys containing 10% Fe and 10% Co. The valence electron configuration was related to the high efficiency of the Mn–Al–Fe powder. Due to the formation of a localized adsorption

bond with the adsorbate molecule, this favors a higher concentration of reactive (hole) sites in the d-band for iron compared to cobalt, favoring a higher adsorption capacity. Moreover, in order to facilitate the creation of hydrogen from water, the zerovalent metals iron (Fe^0) and cobalt (Co^0) act as reactive agents. The azo dye solution's decolorization follows first-order kinetics principles as well. As a result, the high effectiveness of Mn–Al-based alloys observed in decolorization treatments of dyed wastewater, as noted in prior studies, can be adjusted and augmented by moderate alloying with additional transition metals [55]. The ball-milled $\text{Ca}_{65}\text{Al}_{35}$ powder also demonstrated remarkable degrading efficiency and high response rates, removing more than 90% of a 40 mg/L dye solution in less than a minute. These materials may be employed as a low-cost, high-performance decolorizing approach for textile wastewater pretreatments due to their huge surface area, high efficiency, and chemical activity. The reducing capability of Ca serves as the foundation for a mechanism in an aqueous basic media [23]. Table 1 shows some nanoreactives applied in the removal of organic pollutants.

Table 1. List of some nanoreductive materials used in the removal of organic pollutants.

| Alloy Name | Route of Synthesis | Organic Pollutants | Pollutant Concentration | Alloy Dose | pH | Time | Removal | Ref. |
|---------------------------------|-------------------------------|--------------------|-------------------------|------------|-----|---------|---------|------|
| Zerovalent iron | Liquid phase reduction method | Methyl orange | 100 mg/L | 0.5 g/L | 4 | 60 min | 100% | [56] |
| Nanozerovalent iron | Chemically synthesized | Acid black 24 | 100 mg/L | 0.1647 g/L | 6.7 | 80 min | 80% | [57] |
| Nanoscale zerovalent iron | Chemically synthesized | Methylene blue | 70 mg/L | 10 g/L | 7 | 30 min | 72.1% | [58] |
| Iron-based nanoparticles | Green synthesized | Orange II | 5 mg/L | 10 mg/L | 3 | 60 min | 91.12% | [59] |
| Nanoscale zerovalent iron | Liquid phase reduction method | Basic yellow 28 | 100 mg/L | 2 g/L | 2 | 15 min | 99.2% | [60] |
| Zerovalent iron powder | Commercial | Reactive black 5 | 100 mg/L | 0.5 g/L | 3 | 120 min | 100% | [61] |
| Copper nanoparticles | Hydrodynamic cavitation | Methyl orange | 10 mg/L | 40 mg/L | 3 | 20 min | 83% | [62] |
| Zerovalent copper nanoparticles | Chemical reduction | Reactive blue 4 | 15 mg/L | 1 g/L | 3 | 10 min | 90% | [63] |
| Zerovalent cobalt nanoparticles | Galvanic replacement method | Methyl orange | 100 mg/L | 0.5 g/L | 2.5 | 4 min | 99% | [52] |
| AlFeMnTiCr | Ball milled | Direct blue 6 | 200 mg/L | 1 g/L | 7 | 11 min | 100% | [13] |
| AlCrFeMnMg | Ball milled | Direct blue 6 | 200 mg/L | 0.5 g/L | 7 | 6 min | 100% | [39] |
| Mn–Al | Ball milled | Reactive black 5 | 40 mg/L | 2.5 g/L | 3 | 20 min | 100% | [49] |
| Mn–Al | Ball milled | Orange II | 40 mg/L | 2.5 g/L | 3 | 30 min | 100% | [53] |
| Mn–Al | Ball milled | Brilliant green | 150 mg/L | 2.5 g/L | 3 | 75 min | 100% | [54] |
| MnAlFe | Ball milled | Reactive black 5 | 40 mg/L | 2.5 g/L | 3 | 5 min | 100% | [55] |
| Ca–Al | Ball milled | Reactive black 5 | 40 mg | 1 g/L | 6 | 1 min | 100% | [23] |

The use of amorphous alloys is a new approach that has been studied extensively by several research groups. Due to their reduced mass loss, these alloys often exhibit superior corrosion resistance than their crystalline equivalents [64,65]. The amorphous structure of Co-based MG powders is responsible for the rapid degradation of azo dyes by these materials. The potential degradation reactions and mechanisms are depicted in Figure 3 [66].

In comparison with traditional metals, many amorphous alloys have been produced to increase the degradation efficiency of azo dyes in wastewater. Table 2 details the effectiveness and experimental parameters for azo dye removal using amorphous alloys, including the pH solution, initial dye concentration, and alloy dosage. It can be said that amorphous alloys based on Fe, Mg, Co, Al, and Mn are effective at removing various azo dyes from wastewater.

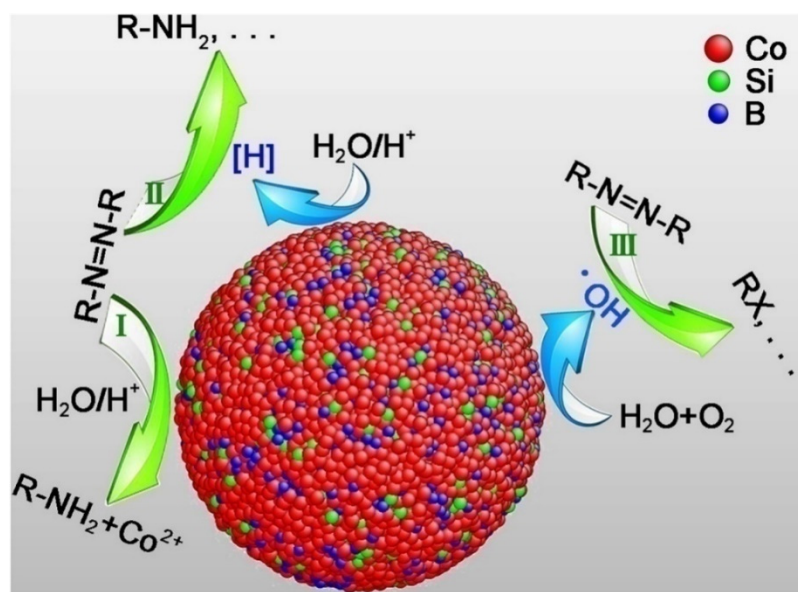


Figure 3. Illustration drawn by Qin et al. of the major reactions occurring in the amorphous alloys and the degradation mechanisms [66].

Table 2. Azo dye degradation with amorphous alloys.

| Alloy Name | Route of Synthesis | Organic Pollutants | Pollutant Concentration | Alloy Dose | pH | Time | Removal | Ref. |
|--------------------------------|------------------------------------|--------------------|-------------------------|------------|-----|---------|---------|------|
| Fe–Si–B amorphous ribbon | Melt spinning | Rhodamine B | 20 mg/L | 0.5 g/L | 3 | 10 min | 100% | [67] |
| Fe–Si–B–Nb amorphous ribbon | Melt spinning | Direct blue 15 | 100 mg/L | 0.03 g/L | - | 60 min | 100% | [68] |
| Fe–Si–B–Cu–Nb amorphous ribbon | Melt spinning | Brilliant red 3B-A | 20 ppm | 2 g/L | 2 | 10 min | 90% | [69] |
| Fe–B–Si–Y | Melt spinning | Methyl orange | 20 mg/L | 4 g/L | 2 | 10 min | 92% | [70] |
| Mg–Cu–Y | Melt spinning + mechanical milling | Direct blue 6 | 0.02 g/L | 1.2 g/L | - | 8 min | 100% | [45] |
| Mg–Zn–Ca | Mechanical milling | Congo red | 200 ppm | 4 g/L | 6.7 | 120 min | 100% | [71] |
| Co–Si–B | Melt spinning + mechanical milling | Acid orange II | 0.2 g/L | 6 g/L | 3 | 2 min | 100% | [66] |

3. Nanophotocatalysis

3.1. Nanocatalysis

3.1.1. Nanomaterials as Photocatalysts

Nanocatalysts are attracting a lot of interest as wastewater treatment materials (especially those nanomaterials made of inorganic substances such as semiconductors and metal oxides). For the purpose of the analysis of oxidation of organic pollutants [72] and antimicrobial effects [73], a variety of nanocatalysts are used in wastewater treatment, including photocatalysts [74,75], electrocatalysts [74], heterojunction photocatalytic materials [76], and Fenton-based catalysts [77] (Table 3).

Due to their extensive and efficient photocatalytic activity for diverse contaminants, nanoparticle photocatalytic reactions, which are based on the interaction of light energy with metallic nanoparticles, are of enormous importance. Usually made of semiconductor metals, these photocatalysts can decompose a variety of persistent organic contaminants found in wastewater, including dyes, detergents, insecticides, and volatile organic compounds [78]. Additionally, semiconductor nanocatalysts are highly efficient at degrading both halogenated and nonhalogenated organic chemicals, as well as certain medications, personal care items, and heavy metals [79]. Semiconductor nanomaterials work well, even at low concentrations, and require relatively benign operating conditions. In the same context, Baaloudj et al. [80] deduced that the photocatalytic performance of catalysts varies,

which was mostly caused by the experimental conditions and, more significantly, by the bandgap, which was crucial to the photocatalytic activity. Depending on the catalyst's color and the components that it is comprised of, the bandgap varies from one catalyst to another. This distinction can be explained by the process in which a semiconductor can be quickly stimulated by light illumination, which absorbs photons with an energy greater than or equal to that of its bandgap energy, and can then be excited to generate electron–hole pairs (e^- and h^+) [81]. After that, O_2 on the surface of the semiconductor will react with the e^- on the conduction band to form $O_2^{\cdot-}$ radicals through a reduction process. The hydroperoxyl radical H_2O^* is then produced by protonation [82]. The trapped electrons, subsequently, combine with these radicals to form hydrogen peroxide H_2O_2 and hydroxide radicals OH^* . The photogenerated valence band holes can react with either water H_2O or the hydroxyl ions OH^- adsorbed on the catalyst surface to produce OH^* radicals, which are powerful oxidants and the primary active oxygen species in the photocatalytic destruction of organic contaminants [83]. Accordingly, it is possible that h^+ makes up a portion of the OH radicals, aiding in the breakdown of organic contaminants [84]. Baaloudj et al. [80] have, therefore, characterized the process by which organic pollutants are broken down to produce electron–hole pairs and active radicle species as follows:

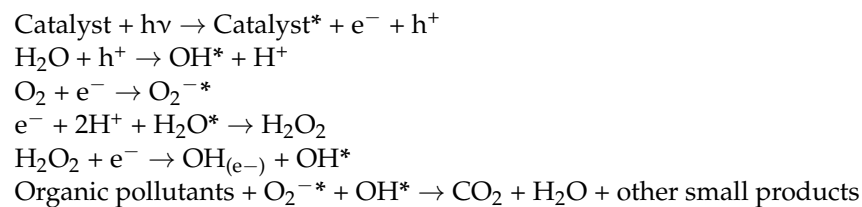


Figure 4 shows a schematic diagram for the proposed mechanism of photocatalysis, depicting the generation of holes (h^+) and electrons (e^-).

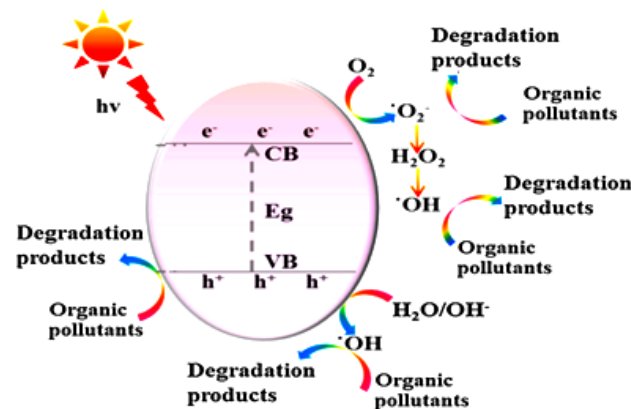


Figure 4. General mechanism of photocatalysis, depicting the generation of holes (h^+) and electrons (e^-) [80].

Several decades ago, the idea of utilizing TiO_2 nanoparticles for photocatalytic dye degradation was proposed [85]. Silver nanoparticles produced by green synthesis have also been applied as photocatalysts to process dyes and other organic compounds [86]. Nanotechnology was not widely used for wastewater treatment at the time, but it is now because of evidence of its great effectiveness [87]. Gold nanoparticles (GNP) with a diameter of 43 nm were employed by Singh et al. to study the photocatalytic degradation of methylene blue (MB). The calculated catalytic degradation at 2 and 3 min was 78.97% and 96.26%, respectively. The fact that GNP's redox potential was decreased to a negative value at the nanoscale explains its catalytic activity [88]. Haque et al. have concentrated on photocatalytic activity, employing La- and Mo-doped TiO_2 hybrid carbon spheres with substantial adsorption capacities, particularly for organic chemicals, such as azo dyes, in light of these characteristics. In 120 min, a 2.0% La-doped TiO_2 and a 1.5% Mo-doped TiO_2 decomposed 94% and 44% of Acid Green 25, respectively. In this case, organics and dyes

were changed into harmless materials by La- and Mo-doped TiO₂. When compared to other dopant concentrations, the photocatalytic activity of TiO₂ with dopant concentrations of 2.0% (La) and 1.5% (Mo) demonstrated the highest effectiveness for the degradation of azo dyes [89].

3.1.2. Nanomaterials as Electrocatalysts

In recent decades, electrocatalysis has undergone significant progress. Numerous fascinating themes in the field of catalysis have arisen as a result of the distinctive characteristics of numerous nanostructures of electrocatalytic materials and their surfaces. Electrocatalysis, a crucial area of catalysis, is a crucial type of catalytic reaction that can transform and store energy through processes involving the transport of electrons. However, because of the extremely complex reaction network, the wide range of reaction selectivity, and the perplexing reaction processes, studying electrocatalysis is extremely difficult. Rare-earth (Gd³⁺, Nd³⁺, and Sm³⁺)-doped cerium oxide has been successfully employed in textile color removal and the decomposition of azo dye RO 107, demonstrating a significant effect on the electrocatalytic activity, according to Rajkumar et al.'s study. The electro-oxidation and electrocatalytic oxidation procedures enable the degradation of high concentration and highly chromoselective dye solutions. The proposed electrochemical degradation process is a successful method of decolorization, according to UV-Vis and FTIR spectral analyses. According to mineralization experiments on RO 107, electrocatalytic oxidation utilizing ceria oxides doped with Gd³⁺, Nd³⁺, and Sm³⁺ increased TOC removal values from 32 to 35.7% after 20 min. The azo bond of the dye structure was the first potentially damaged when the azo bond was attacked, which resulted in the decolorization of the dye. This intermediate was discovered with the GC-MS technique. The intermediates continued to be decomposed into carbon dioxide and water with the aid of the hydroxyl radical and other radicals, which caused the dye solution to become mineralized. When combined with electro-oxidation, cerium-doped Gd³⁺, Nd³⁺, and Sm³⁺ oxides are excellent at removing contaminants from textile dye effluent rapidly. Further research on this method could be performed to find alternative methods for treating wastewater. The findings showed that the cocatalysts for electrocatalytic oxidation processes are Ce_{0.8}Gd_{0.2}O₂, Ce_{0.8}Nd_{0.2}O₂, and Ce_{0.8}Sm_{0.2}O₂. The swift suppression of the electrocharge carriers by the catalyst was the primary electrochemical process responsible for the increased rate. An electron acceptor's favorable function is the production of additional radicals, which effectively degrade the contaminants through the radical chain branching mechanism. To test this at the industrial scale and with other types of organic effluent, more research is required [90].

Using an electrocatalytic vanadium-doped TiO₂ nanocatalyst, Chang et al. examined the degradation of acid red 27 (AR 27). The results showed that AR 27 may be successfully degraded by nano-V/TiO₂ electrodes; the greatest color and total organic carbon (TOC) removal efficiencies reached 99% and 76%, respectively, under 0.10 VT (molar ratio of vanadium to titanium) conditions. A high specific surface area nano-V/TiO₂ electrode aided in electrocatalytic degradation. This electrocatalytic device performed best at a current density of 25 mA cm², and as the current density grew, more oxygen was produced. In this electrocatalytic system, the electrical consumption of the nano-V/TiO₂ electrode and pure-TiO₂ electrode was approximately 0.11 kWh L⁻¹ and 0.02 kWh L⁻¹, respectively. As a result, it can be concluded that the nano-V/TiO₂ electrode had both high degradation and energy-saving qualities. The nano-V/TiO₂ electrode also demonstrated its potential for repeated use [91].

3.1.3. Heterojunction Photocatalytic Material

The heterojunction photocatalytic material, among the different proposed technologies, has the most potential, since it directly uses solar energy for the creation of valuable chemical fuels (hydrogen, hydrocarbon fuels, etc.) as well as the degradation of hazardous pollutants [92–97]. Numerous semiconductors have been researched and produced since Honda and Fujishima's research on photocatalysis in 1972 [98–101]. The spatial separation

of photogenerated electron–hole pairs was shown to enable the appropriately constructed heterojunction photocatalysts to possess enhanced photocatalytic activity. BiVO₄/CeO₂ type-II heterojunction photocatalysts for the photocatalytic degradation of methylene blue (MB), methyl orange (MO), and a combination of MB and MO were synthesized hydrothermally, according to Wetchakun et al. [102]. It was discovered that the pH values of 4.56 for BiVO₄ and 7.33 for CeO₂ corresponded to differing isoelectric points. It has been demonstrated that the difference in isoelectric points between these two semiconductors is advantageous for simultaneously adsorbing cationic and anionic dyes. Particularly, during degrading events, the BiVO₄ and CeO₂ can each preferentially adsorb cationic MB and anionic MO, respectively. Due to the electrostatic repulsion between the surface charges of the photocatalysts and the charges of the dye molecules, the BiVO₄/CeO₂ composite had stronger photocatalytic-degradation activity toward the mixture of MB and MO than the individual BiVO₄ or CeO₂ photocatalysts. The improved electron–hole separation efficiency and potent electrostatic interaction between the composite and the dye molecules were credited for the exceptional activity of the composite photocatalyst. According to this work, the appropriate coupling of two different semiconductors could both increase the effectiveness of electron–hole separation and provide photocatalysts with good adsorption toward both anionic and cationic dyes [76]. Hu et al.'s study of the linked semiconductor Cu₂O/CeO₂ photocatalyst's catalytic activity in the presence of visible light revealed that this heterojunction semiconductor photocatalyst had 20% more photocatalytic degradation of acid orange 7 (AO₇) than pure CeO₂ [103]. The development of p–n junctions was responsible for the highest photoactivity. Li and Yan [104] examined the photocatalytic degradation of Rhodamine B over a Bi₂O₃/CeO₂ catalyst when it was exposed to visible light. The rhodamine B substrate was totally destroyed within 8 h of irradiation, according to their findings, which showed that Bi₂O₃/CeO₂ in a 9:1 molar ratio gave the greatest photodegradation activity. The improved charge carrier lifetime that was attained by using a composite photocatalyst was connected to the improvement in photocatalytic efficiency. The photocatalytic degradation of rhodamine B over ZnO/CeO₂ composite nanofibers was studied by Li et al. [105]. They found that the composite photocatalyst was able to completely degrade the dye substrate within 3 h, while only 17.4% and 82.3% degradation was acquired in the case of pure CeO₂ and pure ZnO, respectively. Li et al. studied the photocatalytic degradation of methylene blue (MB) using Bi₃TaO₇/Ti₃C₂ heterojunctions, and they deduced a removal efficiency of approximately 99% after 2 h [106]. They reported that synergistic effects between Bi₃TaO₇ and Ti₃C₂ improved the photocatalytic performance by enhancing electron–hole pair separation, electronic transmission efficiency, and interfacial charge transfer. They concluded that Ti₃C₂ serves as an “electronic highway”, isolating the photoelectron–hole pairs and enhancing photocatalytic activity. According to their hypothesized photocatalytic mechanism, which is depicted in Figure 5, photogenerated electrons swiftly migrate on Bi₃TaO₇ and congregate on Ti₃C₂ nanosheets. The hydroxyl groups are oxidized by holes gathered on Bi₃TaO₇ to produce OH*, which is an essential oxidant for dye removal. MB can be oxidized immediately by h⁺ to produce the tiny non-toxic molecules H₂O and CO₂ at the same time.

Huang et al. [107] studied the photocatalytic degradation of a Bi₂S₃/Bi₂O₃/Bi₂O₂CO₃ nanocomposite. They demonstrated that this manufactured nanocomposite had superior photocatalytic activity in the breakdown of organic contaminants when exposed to visible light. However, under visible light, these Bi₂S₃/Bi₂O₃/BOC catalysts could remove 99% of HCHO (500 ppm) in 100 min and were able to remove more than 99% of MO in just 60 min. They claimed that the greater light absorption and effective charge separation were responsible for the composite's much better performance, and the mechanism behind this high photocatalytic activity showed that superoxide and holes, as opposed to hydroxyl radicals, dominate the photocatalytic process.

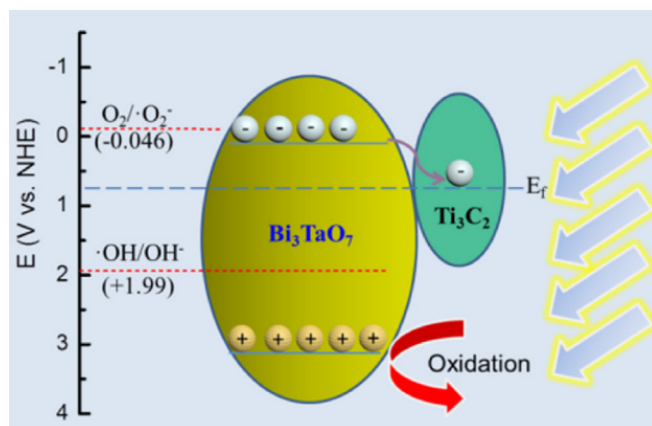


Figure 5. The proposed mechanism for MB removal with BTC-10 under visible light irradiation [107].

According to Low et al., there are at least five basic steps in the photocatalytic process of a semiconductor: (i) the semiconductor's ability to absorb light, (ii) the generation of photogenerated electron–hole pairs, (iii) their transport and recombination, (iv) the adsorption of reactants and the desorption of products, and (v) the activation of redox reactions on their surface (Figure 6) [76].

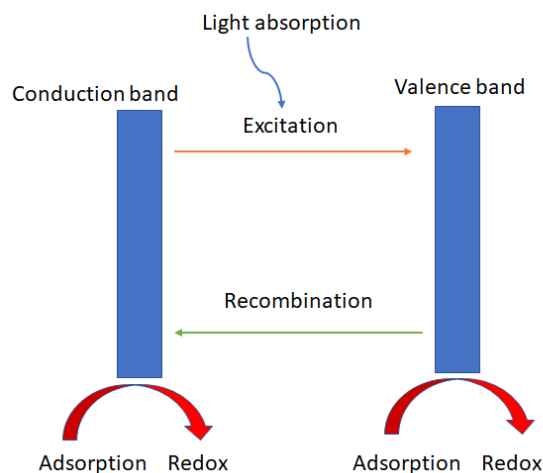


Figure 6. Schema of the typical photocatalytic processes on a heterojunction photocatalytic material.

3.1.4. Nanomaterial-Based Fenton Catalysis

Using the Fenton reaction to improve the effluent's biocompatibility or transform the majority of the organic contaminants into low-molecular-mass carboxylic acids and even CO_2 is one of the most economically advantageous ways to treat wastewater with low-to-medium levels of total organic carbon. By reducing H_2O_2 with Fe II, hydroxyl radicals that are extremely aggressive are produced in the Fenton reaction. As an alternative to Fe II, transition metal ions, such as Cu^+ and Mn^{2+} , can also aid in the process's progress [108]. There have been numerous reports of homogeneous catalysts being effective for the Fenton reaction [109]. The benefit of heterogeneous catalysts is that they make it simpler to separate material from effluent and eventually reuse it. As a result of this, heterogeneous catalysis are viewed as a natural development of homogeneous catalysis [110]. The creation of heterogeneous catalysts for the Fenton reaction has seen a rise in activity in recent years [108,111]. Recently, a review of the development of clays, silicas, and zeolites for heterogeneous Fenton catalysts was published [108]. Activated carbon has been used by numerous research groups either as a heterogeneous catalyst for the Fenton reaction or in other processes. Additionally, it is capable of supporting metals and metal oxides that have catalytic properties for the Fenton reaction (Table 3) [108]. Reviewing the usage of metal

nanoparticles as heterogeneous catalysts for the production of OH radicals from H₂O₂ is also interesting, given the constant increase in the application of the Fenton reaction for the treatment of several industrial effluents. A new generation of nanoparticle-based heterogeneous catalysts has recently been created for the Fenton reaction. Due to the fact that they can have unique characteristics from the macroscopic or bulk forms of the same material, nanoparticles are important [108]. It is well known that some nanoparticles in catalysis have catalytic characteristics that are missing from bulk materials [112]. Additionally, the size, shape, surface structure, and bulk composition of nanocatalysts all have a significant impact on their activity and selectivity.

Table 3. List of nanophotocatalysts in the removal of organic pollutants.

| Alloy | Route of Synthesis | Organic Pollutants | Source of Light | Pollutant Concentration | Catalyst Dose | pH | Time | Removal | Ref. |
|--|----------------------------------|---|-----------------|-------------------------|------------------------------------|---------|----------------------------|--------------------------|-------|
| CuO nanosheets | Room temperature | Alura red Ac | UV | 5 mg/L | 5 mg | Neutral | 6 min | 96.65% | [113] |
| MFe ₂ WO ₆ (M = Co, Ni, Cu, Zn) | Coprecipitation–oxidation method | Methyl red methyl orange Methylene blue bromo green Methyl orange | UV | 10 mg/L | 100 mg | Neutral | 50 min 50 min 50 min | 78% 92% 89% 93% | [114] |
| Cds/CuS | Hydrothermal method | Methyl orange | UV | 10 mg/L | 30 mg | Neutral | 150 min | 93% | [115] |
| α-Bi ₄ V ₂ O ₁₁ | Combustion method | Rhodamine B | UV | 5.106 mol/L | 0.5 g/L | Neutral | 6 min | 100% | [116] |
| TiO ₂ graphene | Chemical Synthesis | Reactive black 5 | UV | 42 ppm | 3 g | Neutral | 40 min | 96% | [117] |
| Al ₂ O ₃ -NP/SnO ₂ | Sol-gel technique | Methyl orange | UV | 20 mg/L | Electrode area 4.5 cm ² | 7 | 50 min | 93.95% | [118] |
| CuO-Co/TiO ₂ | Hydrothermal method | 2-chlorophenol | UV | 50 mg/L | 0.05 g/L | 5 | 210 min | 86% | [119] |
| CuO nanorods | Chemical synthesis | Reactive black 5 | UV | 20 μM | 20 mg | Neutral | 300 min | 98% | [120] |
| Cu/Cu(OH) ₂ | Coprecipitation | Rhodamine B | UV | 100 ppm | 20 mg/L | Neutral | 120 min | 99.99% | [121] |
| Copper nanoparticles | Hydrothermal method | Phenyl red | UV | 10 mg/L | 30 mg | Neutral | 15 min | 99.62% | [122] |

4. Nanoadsorbents

As schematically depicted in Figure 7 [123], several adsorption methods are used to successfully adsorb dye from polluted waters onto the surface of an adsorbent. It should be mentioned that electrostatic attraction, π - π interactions, van der Waals forces, hydrogen bonds, acid–base reactions, and hydrophobic interactions are the key mechanisms controlling the adsorption of water contaminants on adsorbents. The features of nanoparticles that make them appropriate as nanoadsorbents for sequestration of any cleanup procedure are a high splitting coefficient, chemical and thermal stability in the solvent, chemical inertness, high porosity, being easy to remove from a solution after adsorption, sensitive and selective towards the target pollutant, being easily regenerable and reusable numerous times, and easy and inexpensive to manufacture.

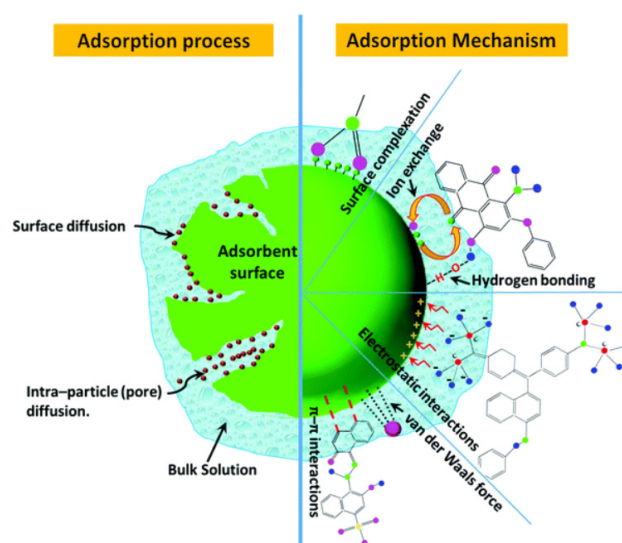


Figure 7. Adsorption processes and mechanisms for dye removal from bulk liquid [123].

The primary intrinsic characteristics of nanoadsorbents, such as their fundamental functional groups and surface modification, are being studied in order to improve their capacity to remove hazardous pollutants throughout the process of wastewater treatment as shown in Tables 4–7. By creating nanocomposites, such as silver/carbon, carbon/titanium oxide, etc., substantial efforts were also made to reduce toxicity. The use of nano-adsorbents in wastewater treatment is the most encouraging method due to their cost-effectiveness, biocompatibility, ease of commercialization, toxic-free method, biodegradability, use of less trained workers, selective separation, ease of recovery, and, most importantly, their high efficacy in removing pollutants.

The following characteristics, including size, shape, surface chemistry, aggregation ability, crystallinity, and chemical reactivity, among others, are crucial in determining how effectively a procedure removes contaminants from an aquatic environment [124].

4.1. Metal Oxide-Based Nanoadsorbents

The inorganic compounds known as metal oxide adsorbents have the distinctive qualities of an increased surface area, high solubility, and reduced production of secondary contaminants. These metal oxide nanoadsorbents can mediate electrostatic interactions due to their charged surfaces, which helps the solute transfer process.

In order to overcome the impacts of fragility, aggregation, and a pressure drop, among other things, a large number of research works on the synthesis of stable nanomaterials and engineering them with the specified functional molecules have been reported. The synthesis of stable nanoceria with amine functionalization was previously reported, and the adsorption procedures used against anionic azo dyes, such as acid yellow 36 and acid yellow 17, were shown to be successful [125,126].

The use of metal oxides to sequester water contaminants has been the subject of numerous studies in recent years (Table 4) [125,127,128]. Their contribution to the environment comes in the form of nanoscale CeO₂ or nanoceria, which functions as a photocatalyst for the decomposition of dyes. Their suitability for the absorption of heavy metal ions is determined by the defined surface features of nanoceria and acceptable electrical charge values [129]. Rajarathinam et al. focused on the synthesis and surface functionalization of nanoceria, and explored their adsorption capability for the removal of azo dye Fenalan Yellow G (FYG) taking these properties into consideration. With an adsorbent dosage of 0.1 g for a dye concentration of 10 mg/L of FYG, the maximum removal of 93.62% was seen after 210 min at a pH of 2.0. According to these results, surface-functionalized nanoceria (sf-gNC) can be used as a substitute material for traditional adsorbents in dye-removal procedures [126].

Studies in this topic have been conducted on how heavy metal ions or colors that are pollutants in wastewater degrade. In order to remove malachite green oxalate (MGO) and hexavalent chromium (Cr) from an aqueous solution, Kumar et al. effectively generated metal oxide nanoparticles, such as ZnO and SnO₂, using a precipitation technique, with specific surface areas of 15.75 and 24.48 m²/g, respectively. ZnO and SnO₂ had 95% and 92% efficiency in decolorizing MGO, respectively. Similarly, Cr adsorbs to ZnO and SnO₂, and they removed 95% and 87% of Cr, respectively [130].

Table 4. Azo dye degradation with oxide-based nanoparticles.

| Alloy Name | Organic Pollutants | Pollutant Concentration | Nanoadsorbent Dosage | pH | Time | Degradation Efficiency | Ref. |
|---|-----------------------------------|-------------------------|----------------------|---------|---------|------------------------|-------|
| TiO ₂ /MgO | Methyl orange alizarin red S | 5 ppm | 0.5 g | Neutral | 90 min | 83.2% 43.8% | [131] |
| CeO ₂ | Methylene blue | 30 mg/L | 200 ppm | Neutral | 60 min | 98% | [132] |
| ZnO/CuO | Congo red | 50 ppm | 50 mg/L | 5.6 | 30 min | 93% | [133] |
| CuO/ γ -Al ₂ O ₃ | Brilliant red X-3B | 0.30 g/L | 5.50 g/L | 8 | 2.50 h | 90.72% | [134] |
| Iron oxide nanoparticles | Metanil yellow Orange II | 20 ppm | 8 mg/L | Neutral | 7 h | 95% 67% | [135] |
| MnO ₂ /SnO ₂ | Calcon dye | 15 mg/L | Film | 3 | 24 h | 93.5% | [136] |
| α -MnO ₂ /TiO ₂ | Coomassie brilliant blue R-250 | 13 mg/L | 1 g/L | 3 | 30 min | 98.35% | [137] |
| Bi ₂ WO ₆ / MnO ₂ | Methylene blue | 10 mg/L | 100 mg/L | 7 | 100 min | 100% | [138] |

4.2. Carbon-Based Nanoadsorbents

Due to the distinctive atomic structure of the carbon atom, carbon materials exhibit a variety of structures and special qualities [139,140]. Carbon materials are classified as zero-dimensional nanomaterials (Buckminster fullerenes and carbon dots), one-dimensional nanomaterials (carbon nanotubes and carbon nanofibers), two-dimensional nanomaterials (graphene), and three-dimensional nanomaterials (carbon sponges) based on their shape, size, and dimensionality [141].

Carbon nanotubes (CNTs) can be found in two-dimensional graphene sheets or three-dimensional nanotubes. They can be divided into two categories based on how many layers or sheets are folded: single-walled CNTs (SWCNTs) and multi-walled CNTs (MWCNTs). SWCNTs play a significant role in clean-up strategies due to their increased surface area, numerous adsorption sites, and other characteristics. The adsorption of a solute on the surface of the adsorbent can be mediated by conventional hydrophobic interactions. As a result, these CNTs are among the adsorbents that have received the most attention in recent years for their capacity to remove a variety of heavy metal ions and organic dyes from wastewater [142].

The maximum adsorption capacity of a given organic pollutant on CNTs was determined by the CNT surface area, surface functional groups on CNTs, the pores in CNT aggregates, surface curvature, and defects of CNT monomers, according to Yang and Xing's review of the aqueous adsorption of organic pollutants using various carbon nanomaterials [143]. The ability of organic pollutants to adhere to CNTs depends in part on the structures and characteristics of the contaminants. The diverse surfaces of CNTs interact in a variety of ways with distinct molecule configurations. To thoroughly analyze the adsorptive interactions between CNTs and organic pollutants, Chen et al. studied the adsorption of contaminants with different physical-chemical properties to three different types of CNTs. They discovered that while the adsorption affinity did not significantly correlate with hydrophobicity, it did rise in the following order: nonpolar aliphatic, nonpolar aromatic, nitroaromatic, and with the number of nitrofunctional groups within the nitroaromatic group [144]. As a result, the type, quantity, and position of functional groups in organic molecules determine how organic pollutant functional groups affect the adsorption of organic pollutants. The order of the substituted groups at a given position following aniline and phenol's affinity for adsorption on CNTs is as follows: nitro group > chloride group > methyl group [145]. Table 5 provides details of the azo dye degradation with some carbon nanotube materials.

Table 5. Azo dye degradation with carbon nanotube materials.

| Alloy Name | Organic Pollutants | Pollutant Concentration | Nano-Sorbent Dosage | pH | Time | Degradation Efficiency | Ref. |
|---|------------------------|-------------------------|------------------------|------|---------|------------------------|-------|
| Multiwall carbon nanotubes (MWCNTs) | Methyl blue | 25 mg/L | 10 mg/L | 6 | 10 min | 99% | [146] |
| Carbon nanotubes grown on carbon fiber | Methylene blue | 5 mg/L | Electrode | 1.83 | 180 min | 100% | [147] |
| ZnO/NiO with multiwall carbon nanotubes | Methyl orange | 50 ppm | 3% NiO:92% ZnO:5% CNTS | 7 | 360 min | 71% | [148] |
| Multiwall carbon nanotubes | Reactive Black 5 | 15 mg/L | 3 g/L | 7 | 60 min | 100% | [149] |
| Single-wall carbon nanotube Ru nanoparticle | Congo red | 0.05 mM | 0.3 mg | 5 | 4 min | 97.5% | [150] |
| Single-wall carbon nanotubes | Reactive yellow dye 15 | 50 mg/L | 0.2 g/L | 3 | 5 min | 179.9mg/g | [151] |
| Carbon nanotubes/alumina | Congo red | 10 mg/L | 15 mg | 2 | 90 min | 96.4% | [152] |

The adsorption capacities of graphene were much higher than those of other adsorbents under similar conditions, making it a promising adsorbent for the removal of heavy metal ions such as Au(III), Pt(IV) [153], Pb(II) [154], Cu(II) [155], Zn(II) [156], Cd(II) [157], and Co(II) [158]. Graphene is one of the most surprising modern carbon allotropes with distinct properties. The most well-known technique of chemical synthesis is the Hummers method [159], which involves oxidizing graphite to create the two-dimensional oxide form of the compound. With a focus on catalytic and degrading activities, the effectiveness of testing graphene oxide (GO) for the elimination of different dyes was thoroughly examined (Table 6) [160]. TiO₂-graphene composites, among a variety of other graphene composites, are frequently employed for the photodegradation of dyes. At the same time, the photocatalytic degradation of dyes, and properties of several metals and metal oxide composites were investigated. The most often studied dye among them for degradation was methylene blue, followed by rhodamine B [160]. Different graphene materials have been used to study dye absorption as well as photocatalytic degradation. Rhodamine B (RB), malachite green (MG), and acriflavine (AF), which are carcinogenic dyes, were applied to highly porous, lightweight graphene oxide foams and high removal capacities were observed of 446, 321 and 228 mg/g, respectively [161]. A simple and affordable lyophilization procedure was used to create the specific 3D GO. Due to the 3D architecture, which is one advantage in terms of its practical use, the foam might be used directly without any preparation, such as in ultrasonication. The excellent antibacterial activity these foams have simultaneously shown against *Escherichia coli* bacteria in aqueous and nutrient growth conditions further suggests their potential for use in water treatment [161].

Table 6. Azo dye degradation with graphene oxide materials.

| Alloy Name | Route of Synthesis | Organic Pollutants | Pollutant Concentration | Nanoadsorbent Dosage | pH | Time | Adsorption Capacity | Ref. |
|--|-------------------------|--|-------------------------|----------------------|-----|--------|----------------------------------|-------|
| Graphene oxide | Modified Hummers method | Acid orange 8 (AO8) and direct red 23 (DR23) | 50 mg/L | 40 mg | 7 | 60 min | AO8 = 25 mg/g and DR23 = 14 mg/g | [162] |
| Graphene oxide and magnetic chitosan | Modified Hummers method | Methyl blue (MB) | 200 mg/L | 0.015 g | 5.3 | 60 min | 95.16 mg/L | [163] |
| Graphene oxide-supported manganese oxide | Modified Hummers method | Reactive black 5 | 60 mg/L | 0.01 g | 3 | 24 h | 87 mg /L | [164] |

4.3. Silica-Based Nanoadsorbents

Sand-like silica is one of the Earth's crust's most abundant components. Owing to its special qualities as a lightweight material, silica is a necessity in the production of electrical and communication devices. Silica is utilized in traditional chromatographic methods to separate the desired solute from a complex mixture. One of the most popular uses for silica is the adsorption of pollutants; it has been widely used to remove colors, heavy metals, and

other contaminants from drinking water [165]. As a result, numerous research studies on the synthesis of silica have been documented. The ability of a synthesized silica nanoparticle (SSN) to remove dye from single and multicomponent (ternary) systems was reported by Mahmoodi et al. Their findings indicated that the SSN, an environmentally benign adsorbent with a high capacity for cationic dye adsorption, would be a good substitute to remove dyes from multicomponent systems (as shown in Table 7) [166].

Table 7. Azo dye degradation with silica-based nanoadsorbents.

| Alloy Name | Organic Pollutants | Pollutant Concentration | Nanoadsorbent Dosage | pH | Time | Degradation Efficiency | Ref. |
|--|--------------------|-------------------------|----------------------|-----|---------|------------------------|-------|
| Nanosilica particles | Methyl orange | 10 mg/L | 10g/3L | 2.5 | 30 min | 100% | [167] |
| Silica nanoparticles | Methyl red dye | 0.05 mM | 10g/L | 7 | 120 min | 95% | [168] |
| Mesoporous silica nanomaterial | Rhodamine B | 20 mg/L | 1g/L | 5.8 | 120 min | 98.92% | [169] |
| Mesoporous silica modified with L-arginine | Crystal violet | 100 ppm | 10 mg | 11 | 30 min | 100% | [170] |
| Porous silicon supporte porous ruthenium nanoparticle system | Condo red | 1 mM | 40 µl | 5 | 60 min | 96% | [171] |
| Titania-coated silica nanocomposite | Safranin-O dye | 17.61 mg/L | 89.80 mg/g | 6.2 | 60 min | 93.29% | [172] |

5. Nanomembranes

Using size exclusion and solution diffusion, nanomembranes, a special type of membrane made of various nanofibers, have been used to remove pollutants based on viruses, inorganic ions, and organic and inorganic nanoparticles from water resources. This method facilitates extremely high elimination rates with condensed fouling propensities, and it also serves as a pretreatment step for reverse osmosis [173]. Numerous studies on membrane nanotechnology have been published in an effort to create multifunctional membranes employing various nanomaterials in various polymer-based membranes [174]. Reverse osmosis, nanofiltration, and other water-treatment methods have used water-porous membranes. A porous support with a composite layer is present in the membrane. The significant composite layer is often composed of a carbon-based material (graphene oxide/CNT) spread in a polymer matrix. As depicted in Figure 8, this results in considerable and prospective advancements in water transport and fouling resistance.

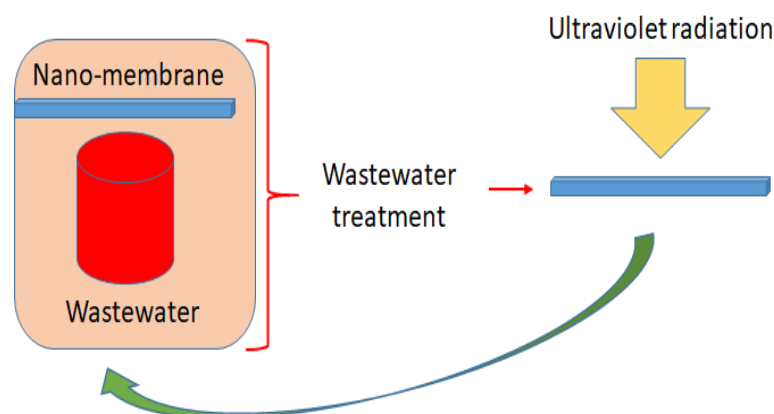


Figure 8. Schema of the nanomembrane procedure for wastewater treatment.

The membranes are commercially available and appropriate for a wide range of uses. However, the effort to create new water resources from sewage calls for membranes with higher productivity and a lower cost related to fouling resistance. Organic substances in water interact with hydrophobic membranes to create membrane fouling. The accumulation of particles on the membrane's surface or inside its pores is the cause of fouling. Almost all membrane processes experience membrane fouling, which is often brought on by precipitation and particle or molecule deposition on the membrane's surface or in its

pores [175]. Increased membrane separation resistances, decreased productivity, and/or altered membrane selectivity are the effects of membrane fouling [176]. Due to fluctuating product quality and poor recovery, this has an impact on the separation factor for the targeted species in the feed. Pore blockage and solute aggregation, which results in a cake development or a gel layer on the membrane surface, in addition to adsorption, which is exacerbated by concentration polarization and convective forces to and through the membrane, are all typical components of the fouling process. Membrane qualities, such as the material from which the membrane is formed, and feed solution properties, such as composition, concentration, pH, and ionic conditions, are the two main groups of factors that affect membrane fouling. In order to remove suspended solids and condition the feed and membrane surface to reduce the tendency for membrane fouling, pretreatments of feed that have an impact on the feed's properties in membrane systems are crucial.

A high specific surface area and high porosity with small pores are two distinctive characteristics of electrospun nanofiber membranes. The development of an efficient technology for processing wastewater dyes has been the subject of numerous studies. A variety of techniques have been developed to remove synthetic colors from water and wastewater to reduce their environmental impact. Adsorption on inorganic or organic matrices, color removal via photocatalysis, oxidation, microbiological or enzymatic breakdown, etc., are some of the technologies used [177]. One of the most efficient and financially viable methods for removing textile colours from wastewater is adsorption [178].

The surface area and structure of an adsorbent are its most crucial characteristics. Additionally, the adsorbent surface's polarity and chemical make-up may affect the attractive forces that bind the adsorbent to the adsorbate [179]. Due to these characteristics, electrospun nanofiber membranes have been utilized to filter out heavy metal ions [180,181] and dye molecules from textile effluent [182]. The sorption potential of electrospun TPU and PVA nanofiber membranes was assessed by Akduman et al. These nanofiber membranes' large surface areas per unit volume make them perfectly suited for the physical adsorption-based removal of certain materials. The hydrophobic structure of TPU nanofiber membranes, however, resulted in relatively low adsorptions. However, PVA nanofiber membranes, in particular those that were BTCA cross-linked, performed well when it came to the sorption of the dye Reactive Red 141. The highest possible sorption capacity was 88.31 mg/g. The sorption capacity was reduced, nevertheless, as the heat setting temperature rose from 110 °C to 130 °C. The membranes' volume was also extremely low following the drying process and adsorption process. Thus, these materials might offer a new method for removing colour molecules from textile effluent (Table 8) [183].

Table 8. Azo dye degradation with nanomembranes.

| Nanomembranes | Organic Pollutants | References |
|--|--|------------|
| Chitosan | Methyl viologen, methylene blue, methyl orange, orange G, rose bengal, brilliant blue and methyl red | [184] |
| Nanofiltration surfactant (NFS) | Methyl violet, methyl blue and acid orange 74 | [185] |
| Polyetherimide (PEI)-based nanofiltration (NF) | Reactive red | [186] |
| Hydracore 10 and hydracore 50 | Cibacron yellow S-3R | [187] |
| Polyamide NF | Anthraquinone dyes | [188] |
| ZrO ₂ | Dimethyl formamide | [189] |

6. Conclusions and Future Perspectives

Freshwater is obviously necessary for all living things, and if wastewater is properly treated, it can also be used again. Azo dyes are the primary source of wastewater produced by the textile sector. This calls for the necessity for an efficient azo dye wastewater treatment. Various nanomaterials were described in this review paper for the removal of azo dye from wastewater. The nanoreductive degradation by metallic amorphous or nanocrystalline alloys favored azo bond cleavage. There were also some parameters that influenced treatment results such as the pH, temperature, and dye-nanomaterial dosage. Likewise, catalysis processes with nanomaterials based on photocatalysis (including heterojunction

materials), electrocatalysis, or Fenton catalysis were an alternative. One of the remaining problems after azo dye degradation was related to the formation of aromatic compounds. In order to remove these amines or phenoles, but also as an option to eliminate directly the azo molecules, one option is the use of nanosorbents. In this review, we provided scientific literature about some nanoadsorbents, which were metal oxide-based, carbon-based (including graphene), and silica-based. Furthermore, we discussed the use of nanomembranes to separate water pollutants using solution diffusion and/or size reduction.

The majority of research has been performed at a small scale in laboratories. These methods need to be scaled up to the industry scale. In conclusion, hotspots for scientific research could include real-time monitoring, material toxicity, risk analysis, mechanism elucidation, the potential for reuse, fouling problems, continuous flow operations, a lack of commercialization, and the pursuit of new-generation versatile nanomaterials, among others.

The most thoroughly studied nanomaterials include metal oxide NPs, such as TiO₂ and ZnO, CNTs, and nanocomposites. There was also a thorough explanation of how they were used in the treatment of wastewater and water. Nanomaterials have a lot of potential for cleaning water and wastewater, given how quickly they are being created and deployed. The difficulties caused by nanomaterials must be resolved through additional research. Only a few types of nanomaterial have seen widespread commercial use. The economic effectiveness of nanomaterials should be the main topic of future research. With the extensive and regular usage of nanomaterials in water and sewage systems, the likelihood of the toxicity of nanomaterials affecting the environment and human health is also increasing. There is evidence that certain nanomaterials can have detrimental effects on the environment and human health. However, the present recommendations for assessing the dangers of nanomaterials are insufficient and weak. Nanomaterials' toxicity needs to be thoroughly assessed before they can be used in practical applications. Additionally, there are numerous obstacles to overcome before universal or acknowledged standards are created for calculating and evaluating nanoparticles in water and sewage systems. As each nanomaterial performs differently, it is challenging to select those that warrant additional research and development. Future assessments of nanoparticles' efficacy in treating water and wastewater will be necessary.

Author Contributions: Conceptualization, J.-J.S. and F.M.A.; methodology, J.S. and E.P.; formal analysis, W.B.M. and L.E.; investigation, W.B.M. and L.E.; writing—original draft preparation, M.K. and W.B.M.; writing—review and editing, J.-J.S.; supervision, J.-J.S. and M.K. All authors have read and agreed to the published version of the manuscript.

Funding: This research was funded by the University of Girona, project UNIGE-01 and Spanish MCIN, project PID2020-112975GB-I00.

Institutional Review Board Statement: Not applicable in this study.

Informed Consent Statement: Not applicable.

Data Availability Statement: Data can be requested from the authors.

Acknowledgments: We acknowledge the technical support of the Serveis Tècnics de Recerca of the University of Girona.

Conflicts of Interest: The authors declare no conflict of interest.

References

1. Saratale, R.G.; Saratale, G.D.; Chang, J.S.; Govindwar, S.P. Bacterial Decolorization and Degradation of Azo Dyes: A Review. *J. Taiwan Inst. Chem. Eng.* **2011**, *42*, 138–157. [[CrossRef](#)]
2. Marañón, E.; Castrillón, L.; Fernández-Nava, Y.; Fernández-Méndez, A.; Fernández-Sánchez, A. Colour, Turbidity and COD Removal from Old Landfill Leachate by Coagulation-Flocculation Treatment. *Waste Manag. Res.* **2010**, *28*, 731–737. [[CrossRef](#)] [[PubMed](#)]
3. Van Pham, T.; Phuoc, V.M.; Van Nguyen, D.; Koyama, J. Treatment Efficiency of a Combination of Alternative Technologies in Removing Pollutants from Pesticide Containing Wastewater. *Environ. Eng. Res.* **2021**, *26*, 63. [[CrossRef](#)]

4. Huang, F.; Chen, L.; Wang, H.; Feng, T.; Yan, Z. Degradation of Methyl Orange by Atmospheric DBD Plasma: Analysis of the Degradation Effects and Degradation Path. *J. Electrostat.* **2012**, *70*, 43–47. [[CrossRef](#)]
5. Bali, U.; Çatalkaya, E.Ç.; Şengül, F. Photochemical Degradation and Mineralization of Phenol: A Comparative Study. *J. Environ. Sci. Health Part A* **2003**, *38*, 2259–2275. [[CrossRef](#)] [[PubMed](#)]
6. Utari, A.W.; Herdiansyah, H. Filtration as a Water Treatment Method: Used to Remove TSS and COD in Household Wastewater. *AIP Conf. Proc.* **2020**, *2245*, 060004. [[CrossRef](#)]
7. Arslan-Alaton, I.; Seremet, O. Advanced Treatment of Biotreated Textile Industry Wastewater with Ozone, Virgin/Ozonated Granular Activated Carbon and Their Combination. *J. Environ. Sci. Health Part A* **2004**, *39*, 1681–1694. [[CrossRef](#)] [[PubMed](#)]
8. Afrin, S.; Shuvo, H.R.; Sultana, B.; Islam, F.; Rus'd, A.A.; Begum, S.; Hossain, M.N. The Degradation of Textile Industry Dyes Using the Effective Bacterial Consortium. *Heliyon* **2021**, *7*, e08102. [[CrossRef](#)]
9. Yaqoob, A.A.; Parveen, T.; Umar, K.; Ibrahim, M.N.M. Role of Nanomaterials in the Treatment of Wastewater: A Review. *Water* **2020**, *12*, 495. [[CrossRef](#)]
10. Amin, M.T.; Alazba, A.A.; Manzoor, U. A Review of Removal of Pollutants from Water/Wastewater Using Different Types of Nanomaterials. *Adv. Mater. Sci. Eng.* **2014**, *2014*, 825910. [[CrossRef](#)]
11. Paramasivam, G.; Palem, V.V.; Sundaram, T.; Sundaram, V.; Kishore, S.C.; Bellucci, S. Nanomaterials: Synthesis and Applications in Theranostics. *Nanomaterials* **2021**, *11*, 3228. [[CrossRef](#)] [[PubMed](#)]
12. Tang, X.; Zhang, Q.; Liu, Z.; Pan, K.; Dong, Y.; Li, Y. Removal of Cu(II) by Loofah Fibers as a Natural and Low-Cost Adsorbent from Aqueous Solutions. *J. Mol. Liq.* **2014**, *199*, 401–407. [[CrossRef](#)]
13. Wu, S.; Pan, Y.; Wang, N.; Lu, T.; Dai, W. Azo Dye Degradation Behavior of AlFeMnTiM (M = Cr, Co, Ni) High-Entropy Alloys. *Int. J. Miner. Metall. Mater.* **2019**, *26*, 124–132. [[CrossRef](#)]
14. Mir, N.; Khan, A.; Umar, K.; Muneer, M. Photocatalytic Study of a Xanthene Dye Derivative, Phloxine B in Aqueous Suspension of TiO₂: Adsorption Isotherm and Decolourization Kinetics. *Energy Environ. Focus* **2013**, *2*, 208–216. [[CrossRef](#)]
15. Fang, X.; Li, J.; Li, X.; Pan, S.; Zhang, X.; Sun, X.; Shen, J.; Han, W.; Wang, L. Internal Pore Decoration with Poly-dopamine Nanoparticle on Polymeric Ultrafiltration Membrane for Enhanced Heavy Metal Removal. *Chem. Eng. J.* **2017**, *314*, 38–49. [[CrossRef](#)]
16. Sekoai, P.T.; Ouma, C.N.M.; du Preez, S.P.; Modisha, P.; Engelbrecht, N.; Bessarabov, D.G.; Ghimire, A. Application of Nanoparticles in Biofuels: An Overview. *Fuel* **2019**, *237*, 380–397. [[CrossRef](#)]
17. Ge, Y.; Li, Z. Application of Lignin and Its Derivatives in Adsorption of Heavy Metal Ions in Water: A Review. *ACS Sustain. Chem. Eng.* **2018**, *6*, 7181–7192. [[CrossRef](#)]
18. Sun, R.; Yang, J.; Huang, R.; Wang, C. Controlled Carbonization of Microplastics Loaded Nano Zero-Valent Iron for Catalytic Degradation of Tetracycline. *Chemosphere* **2022**, *303*, 135123. [[CrossRef](#)]
19. Hassan, S.E.D.; Fouda, A.; Saied, E.; Farag, M.M.S.; Eid, A.M.; Barghoth, M.G.; Awad, M.A.; Hamza, M.F.; Awad, M.F. Rhizopus Oryzae-Mediated Green Synthesis of Magnesium Oxide Nanoparticles (MgO-NPs): A Promising Tool for Antimicrobial, Mosquitocidal Action, and Tanning Effluent Treatment. *J. Fungi* **2021**, *7*, 372. [[CrossRef](#)]
20. Sukhanova, A.; Bozrova, S.; Sokolov, P.; Berestovoy, M.; Karaulov, A.; Nabiev, I. Dependence of Nanoparticle Toxicity on Their Physical and Chemical Properties. *Nanoscale Res. Lett.* **2018**, *13*, 44. [[CrossRef](#)]
21. Zwiehoff, S.; Johnny, J.; Behrends, C.; Landmann, A.; Mentzel, F.; Bäumer, C.; Kröniger, K.; Rehbock, C.; Timmermann, B.; Barcikowski, S.; et al. Enhancement of Proton Therapy Efficiency by Noble Metal Nanoparticles Is Driven by the Number and Chemical Activity of Surface Atoms. *Small* **2022**, *18*, 2106383. [[CrossRef](#)] [[PubMed](#)]
22. Miernicki, M.; Hofmann, T.; Eisenberger, I.; von der Kammer, F.; Praetorius, A. Legal and Practical Challenges in Classifying Nanomaterials According to Regulatory Definitions. *Nat. Nanotechnol.* **2019**, *14*, 208–216. [[CrossRef](#)] [[PubMed](#)]
23. Ben Mbarek, W.; Pineda, E.; Escoda, L.; Suñol, J.J.; Khitouni, M. High Efficiency Decolorization of Azo Dye Reactive Black 5 by Ca-Al Particles. *J. Environ. Chem. Eng.* **2017**, *5*, 6107–6113. [[CrossRef](#)]
24. Khalil, A.M.E.; Eljamal, O.; Amen, T.W.M.; Sugihara, Y.; Matsunaga, N. Optimized Nano-Scale Zero-Valent Iron Supported on Treated Activated Carbon for Enhanced Nitrate and Phosphate Removal from Water. *Chem. Eng. J.* **2017**, *309*, 349–365. [[CrossRef](#)]
25. Sun, L.; Wang, C.; Ji, M.; Kong, X. Treatment of Mixed Chemical Wastewater and the Agglomeration Mechanism via an Internal Electrolysis Filter. *Chem. Eng. J.* **2013**, *215–216*, 50–56. [[CrossRef](#)]
26. Xiong, Z.; Lai, B.; Yang, P.; Zhou, Y.; Wang, J.; Fang, S. Comparative Study on the Reactivity of Fe/Cu Bimetallic Particles and Zero Valent Iron (ZVI) under Different Conditions of N₂, Air or without Aeration. *J. Hazard. Mater.* **2015**, *297*, 261–268. [[CrossRef](#)]
27. Bigg, T.; Judd, S.J. Kinetics of Reductive Degradation of Azo Dye by Zero-Valent Iron. *Process Saf. Environ. Prot.* **2001**, *79*, 297–303. [[CrossRef](#)]
28. Elliott, D.W.; Zhang, W.X. Field Assessment of Nanoscale Bimetallic Particles for Groundwater Treatment. *Environ. Sci. Technol.* **2001**, *35*, 4922–4926. [[CrossRef](#)]
29. Zhang, W.X.; Wang, C.B.; Lien, H.L. Treatment of Chlorinated Organic Contaminants with Nanoscale Bimetallic Particles. *Catal. Today* **1998**, *40*, 387–395. [[CrossRef](#)]
30. Lien, H.-L.; Zhang, W. Transformation of Chlorinated Methanes by Nanoscale Iron Particles. *J. Environ. Eng.* **1999**, *125*, 1042–1047. [[CrossRef](#)]
31. Grittini, C.; Malcomson, M.; Fernando, Q.; Korte, N. Rapid Dechlorination of Polychlorinated Biphenyls on the Surface of a Pd/Fe Bimetallic System. *Environ. Sci. Technol.* **2002**, *29*, 2898–2900. [[CrossRef](#)] [[PubMed](#)]

32. Lien, H.; Zhang, W. Hydrodechlorination of Chlorinated Ethanes by Nanoscale Pd/Fe Bimetallic Particles. *ASCE* **2005**, *131*, 4–10. [[CrossRef](#)]
33. Xu, Y.; Zhang, W.X. Subcolloidal Fe/Ag Particles for Reductive Dehalogenation of Chlorinated Benzenes. *Ind. Eng. Chem. Res.* **2000**, *39*, 2238–2244. [[CrossRef](#)]
34. Tee, Y.H.; Bachas, L.; Bhattacharyya, D. Degradation of Trichloroethylene and Dichlorobiphenyls by Iron-Based Bimetallic Nanoparticles. *J. Phys. Chem. C* **2009**, *113*, 9454–9464. [[CrossRef](#)]
35. Barnes, R.J.; Riba, O.; Gardner, M.N.; Scott, T.B.; Jackman, S.A.; Thompson, I.P. Optimization of Nano-Scale Nickel/Iron Particles for the Reduction of High Concentration Chlorinated Aliphatic Hydrocarbon Solutions. *Chemosphere* **2010**, *79*, 448–454. [[CrossRef](#)]
36. Barnes, R.J.; Riba, O.; Gardner, M.N.; Singer, A.C.; Jackman, S.A.; Thompson, I.P. Inhibition of Biological TCE and Sulphate Reduction in the Presence of Iron Nanoparticles. *Chemosphere* **2010**, *80*, 554–562. [[CrossRef](#)] [[PubMed](#)]
37. Schrick, B.; Blough, J.L.; Jones, A.D.; Mallouk, T.E. Hydrodechlorination of Trichloroethylene to Hydrocarbons Using Bimetallic Nickel-Iron Nanoparticles. *Chem. Mater.* **2002**, *14*, 5140–5147. [[CrossRef](#)]
38. Miracle, D.B.; Senkov, O.N. A Critical Review of High Entropy Alloys and Related Concepts. *Acta Mater.* **2017**, *122*, 448–511. [[CrossRef](#)]
39. Wu, S.; Pan, Y.; Lu, J.; Wang, N.; Dai, W.; Lu, T. Effect of the Addition of Mg, Ti, Ni on the Decoloration Performance of AlCrFeMn High Entropy Alloy. *J. Mater. Sci. Technol.* **2019**, *35*, 1629–1635. [[CrossRef](#)]
40. Qin, P.; Yang, Y.; Zhang, X.; Niu, J.; Yang, H.; Tian, S.; Zhu, J.; Lu, M. Highly Efficient, Rapid, and Simultaneous Removal of Cationic Dyes from Aqueous Solution Using Monodispersed Mesoporous Silica Nanoparticles as the Adsorbent. *Nanomaterials* **2017**, *8*, 4. [[CrossRef](#)]
41. Jiang, L.; Jiang, H.; Lu, Y.; Wang, T.; Cao, Z.; Li, T. Mechanical Properties Improvement of AlCrFeNi₂Ti_{0.5} High Entropy Alloy through Annealing Design and Its Relationship with Its Particle-Reinforced Microstructures. *J. Mater. Sci. Technol.* **2015**, *31*, 397–402. [[CrossRef](#)]
42. Dolique, V.; Thomann, A.L.; Brault, P.; Tessier, Y.; Gillon, P. Thermal Stability of AlCoCrCuFeNi High Entropy Alloy Thin Films Studied by In-Situ XRD Analysis. *Surf. Coat. Technol.* **2010**, *204*, 1989–1992. [[CrossRef](#)]
43. Shi, Y.; Yang, B.; Xie, X.; Brechtel, J.; Dahmen, K.A.; Liaw, P.K. Corrosion of AlXCoCrFeNi High-Entropy Alloys: Al-Content and Potential Scan-Rate Dependent Pitting Behavior. *Corros. Sci.* **2017**, *119*, 33–45. [[CrossRef](#)]
44. Chou, Y.L.; Wang, Y.C.; Yeh, J.W.; Shih, H.C. Pitting Corrosion of the High-Entropy Alloy Co_{1.5}CrFeNi_{1.5}Ti_{0.5}Mo_{0.1} in Chloride-Containing Sulphate Solutions. *Corros. Sci.* **2010**, *52*, 3481–3491. [[CrossRef](#)]
45. Luo, X.; Li, R.; Zong, J.; Zhang, Y.; Li, H.; Zhang, T. Enhanced Degradation of Azo Dye by Nanoporous-Copper-Decorated Mg-Cu-Y Metallic Glass Powder through Dealloying Pretreatment. *Appl. Surf. Sci.* **2014**, *305*, 314–320. [[CrossRef](#)]
46. Dong, H.; Jiang, Z.; Zhang, C.; Deng, J.; Hou, K.; Cheng, Y.; Zhang, L.; Zeng, G. Removal of Tetracycline by Fe/Ni Bimetallic Nanoparticles in Aqueous Solution. *J. Colloid Interface Sci.* **2018**, *513*, 117–125. [[CrossRef](#)]
47. Safavi, A.; Momeni, S. Highly Efficient Degradation of Azo Dyes by Palladium/Hydroxyapatite/Fe₃O₄ Nanocatalyst. *J. Hazard. Mater.* **2012**, *201–202*, 125–131. [[CrossRef](#)]
48. Crane, R.A.; Scott, T.B. Nanoscale Zero-Valent Iron: Future Prospects for an Emerging Water Treatment Technology. *J. Hazard. Mater.* **2012**, *211–212*, 112–125. [[CrossRef](#)]
49. Ben Mbarek, W.; Azabou, M.; Pineda, E.; Fiol, N.; Escoda, L.; Suñol, J.J.; Khitouni, M. Rapid Degradation of Azo-Dye Using Mn-Al Powders Produced by Ball-Milling. *RSC Adv.* **2017**, *7*, 12620–12628. [[CrossRef](#)]
50. Wang, P.; Wang, J.Q.; Li, H.; Yang, H.; Huo, J.; Wang, J.; Chang, C.; Wang, X.; Li, R.W.; Wang, G. Fast Decolorization of Azo Dyes in Both Alkaline and Acidic Solutions by Al-Based Metallic Glasses. *J. Alloys Compd.* **2017**, *701*, 759–767. [[CrossRef](#)]
51. Mao, A.; Ding, P.; Quan, F.; Zhang, T.; Ran, X.; Li, Y.; Jin, X.; Gu, X. Effect of Aluminum Element on Microstructure Evolution and Properties of Multicomponent Al-Co-Cr-Cu-Fe-Ni Nanoparticles. *J. Alloys Compd.* **2018**, *735*, 1167–1175. [[CrossRef](#)]
52. Sha, Y.; Mathew, I.; Cui, Q.; Clay, M.; Gao, F.; Zhang, X.J.; Gu, Z. Rapid Degradation of Azo Dye Methyl Orange Using Hollow Cobalt Nanoparticles. *Chemosphere* **2016**, *144*, 1530–1535. [[CrossRef](#)] [[PubMed](#)]
53. AboliGhasemabadi, M.; Mbarek, W.B.; Casabella, O.; Roca-Bisbe, H.; Pineda, E.; Escoda, L.; Suñol, J.J. Application of Mechanically Alloyed MnAl Particles to De-Colorization of Azo Dyes. *J. Alloys Compd.* **2018**, *741*, 240–245. [[CrossRef](#)]
54. AboliGhasemabadi, M.; Ben Mbarek, W.; Cerrillo-Gil, A.; Roca-Bisbe, H.; Casabella, O.; Blázquez, P.; Pineda, E.; Escoda, L.; Suñol, J.J. Azo-Dye Degradation by Mn–Al Powders. *J. Environ. Manag.* **2020**, *258*, 110012. [[CrossRef](#)] [[PubMed](#)]
55. Mbarek, W.B.; Saurina, J.; Escoda, L.; Pineda, E.; Khitouni, M.; Suñol, J.-J. Effects of the Addition of Fe, Co on the Azo Dye Degradation Ability of Mn-Al Mechanically Alloyed Powders. *Metals* **2020**, *10*, 1578. [[CrossRef](#)]
56. Fan, J.; Guo, Y.; Wang, J.; Fan, M. Rapid Decolorization of Azo Dye Methyl Orange in Aqueous Solution by Nanoscale Zerovalent Iron Particles. *J. Hazard. Mater.* **2009**, *166*, 904–910. [[CrossRef](#)]
57. Shu, H.Y.; Chang, M.C.; Yu, H.H.; Chen, W.H. Reduction of an Azo Dye Acid Black 24 Solution Using Synthesized Nanoscale Zerovalent Iron Particles. *J. Colloid Interface Sci.* **2007**, *314*, 89–97. [[CrossRef](#)]
58. Hamdy, A.; Mostafa, M.K.; Nasr, M. Zero-Valent Iron Nanoparticles for Methylene Blue Removal from Aqueous Solutions and Textile Wastewater Treatment, with Cost Estimation. *Water Sci. Technol.* **2018**, *78*, 367–378. [[CrossRef](#)]
59. Luo, F.; Yang, D.; Chen, Z.; Megharaj, M.; Naidu, R. The Mechanism for Degrading Orange II Based on Adsorption and Reduction by Ion-Based Nanoparticles Synthesized by Grape Leaf Extract. *J. Hazard. Mater.* **2015**, *296*, 37–45. [[CrossRef](#)]

60. Poursaberi, T.; Hassanisadi, M.; Nourmohammadian, F. Application of Synthesized Nanoscale Zero-Valent Iron in the Treatment of Dye Solution Containing Basic Yellow 28. *Prog. Color. Color. Coat.* **2012**, *5*, 35–40. [[CrossRef](#)]
61. Satapanajaru, T.; Chompuchan, C.; Suntornchot, P.; Pengthamkeerati, P. Enhancing Decolorization of Reactive Black 5 and Reactive Red 198 during Nano Zerovalent Iron Treatment. *Desalination* **2011**, *266*, 218–230. [[CrossRef](#)]
62. Li, P.; Song, Y.; Wang, S.; Tao, Z.; Yu, S.L.; Liu, Y.A. Enhanced decolorization of methyl orange using zero-valent copper nanoparticles under assistance of hydrodynamic cavitation. *Ultrason. Chem.* **2015**, *22*, 132–138. [[CrossRef](#)] [[PubMed](#)]
63. Marcelo, C.R.; Puiatti, G.A.; Nascimento, M.A.; Oliveira, A.F.; Lopes, R.P. Degradation of the Reactive Blue 4 Dye in Aqueous Solution Using Zero-Valent Copper Nanoparticles. *J. Nanomater.* **2018**, *2018*, 4642038. [[CrossRef](#)]
64. Schroers, J. Bulk Metallic Glasses. *Phys. Today* **2013**, *66*, 32. [[CrossRef](#)]
65. Sun, S.P.; Wang, K.Y.; Rajarathnam, D.; Hatton, T.A.; Chung, T.S. Polyamide-Imide Nanofiltration Hollow Fiber Membranes with Elongation-Induced Nano-Pore Evolution. *AIChE J.* **2010**, *56*, 1481–1494. [[CrossRef](#)]
66. Qin, X.D.; Zhu, Z.W.; Liu, G.; Fu, H.M.; Zhang, H.W.; Wang, A.M.; Li, H.; Zhang, H.F. Ultrafast Degradation of Azo Dyes Catalyzed by Cobalt-Based Metallic Glass. *Sci. Rep.* **2015**, *5*, 18226. [[CrossRef](#)]
67. Wang, X.; Pan, Y.; Zhu, Z.; Wu, J. Efficient Degradation of Rhodamine B Using Fe-Based Metallic Glass Catalyst by Fenton-like Process. *Chemosphere* **2014**, *117*, 638–643. [[CrossRef](#)]
68. Deng, Z.; Zhang, X.H.; Chan, K.C.; Liu, L.; Li, T. Fe-Based Metallic Glass Catalyst with Nanoporous Surface for Azo Dye Degradation. *Chemosphere* **2017**, *174*, 76–81. [[CrossRef](#)]
69. Jia, Z.; Liang, S.X.; Zhang, W.C.; Wang, W.M.; Yang, C.; Zhang, L.C. Heterogeneous Photo Fenton-like Degradation of Cibacron Brilliant Red 3B-A Dye Using Amorphous Fe₇₈Si₉B₁₃ and Fe_{73.5}Si_{13.5}B₉Cu₁Nb₃ Alloys: The Influence of Adsorption. *J. Taiwan Inst. Chem. Eng.* **2017**, *71*, 128–136. [[CrossRef](#)]
70. Xie, S.; Huang, P.; Kruzic, J.J.; Zeng, X.; Qian, H. A Highly Efficient Degradation Mechanism of Methyl Orange Using Fe-Based Metallic Glass Powders. *Sci. Rep.* **2016**, *6*, 21947. [[CrossRef](#)]
71. Ramya, M.; Karthika, M.; Selvakumar, R.; Raj, B.; Ravi, K.R. A Facile and Efficient Single Step Ball Milling Process for Synthesis of Partially Amorphous Mg-Zn-Ca Alloy Powders for Dye Degradation. *J. Alloys Compd.* **2017**, *696*, 185–192. [[CrossRef](#)]
72. Ma, H.; Wang, H.; Na, C. Microwave-Assisted Optimization of Platinum-Nickel Nanoalloys for Catalytic Water Treatment. *Appl. Catal. B Environ.* **2015**, *163*, 198–204. [[CrossRef](#)]
73. Chaturvedi, S.; Dave, P.N.; Shah, N.K. Applications of Nano-Catalyst in New Era. *J. Saudi Chem. Soc.* **2012**, *16*, 307–325. [[CrossRef](#)]
74. Dutta, A.K.; Maji, S.K.; Adhikary, B. γ -Fe₂O₃ Nanoparticles: An Easily Recoverable Effective Photo-Catalyst for the Degradation of Rose Bengal and Methylene Blue Dyes in the Waste-Water Treatment Plant. *Mater. Res. Bull.* **2014**, *49*, 28–34. [[CrossRef](#)]
75. Luo, Y.; Wang, Y.; Hua, F.; Xue, M.; Xie, X.; Xie, Y.; Yu, Y.; Shouhan, Z.; Longshuai, Y.; Zuozhu, X.; et al. Adsorption and photodegradation of reactive red 120 with nickel-iron-layered double hydroxide/biochar composites. *J. Hazard. Mater.* **2023**, *443*, 130300. [[CrossRef](#)] [[PubMed](#)]
76. Low, J.; Yu, J.; Jaroniec, M.; Wageh, S.; Al-Ghamdi, A.A. Heterojunction Photocatalysts. *Adv. Mater.* **2017**, *29*, 1601694. [[CrossRef](#)]
77. Kurian, M.; Nair, D.S. Heterogeneous Fenton Behavior of Nano Nickel Zinc Ferrite Catalysts in the Degradation of 4-Chlorophenol from Water under Neutral Conditions. *J. Water Process Eng.* **2015**, *8*, e37–e49. [[CrossRef](#)]
78. Lin, S.T.; Thirumavalavan, M.; Jiang, T.Y.; Lee, J.F. Synthesis of ZnO/Zn Nano Photocatalyst Using Modified Polysaccharides for Photodegradation of Dyes. *Carbohydr. Polym.* **2014**, *105*, 1–9. [[CrossRef](#)]
79. Adeleye, A.S.; Conway, J.R.; Garner, K.; Huang, Y.; Su, Y.; Keller, A.A. Engineered Nanomaterials for Water Treatment and Remediation: Costs, Benefits, and Applicability. *Chem. Eng. J.* **2016**, *286*, 640–662. [[CrossRef](#)]
80. Baaloudj, O.; Assadi, I.; Nasrallah, N.; El Jery, A.; Khezami, L.; Assadi, A.A. Simultaneous Removal of Antibiotics and Inactivation of Antibiotic-Resistant Bacteria by Photocatalysis: A Review. *J. Water Process Eng.* **2021**, *42*, 102089. [[CrossRef](#)]
81. Reyes, C.; Fernandez, J.; Freer, J.; Mondaca, M.A.; Zaror, C.; Malato, S.; Mansilla, H.D. Degradation and inactivation of tetracycline by TiO₂ photocatalysis. *J. Photochem. Photobiol. A Chem.* **2006**, *184*, 141–146. [[CrossRef](#)]
82. Dong, S.; Cui, L.; Zhang, W.; Xia, L.; Zhou, S.; Russell, C.K.; Fan, M.; Feng, J.; Sun, J. Double-shelled ZnSnO₃ hollow cubes for efficient photocatalytic degradation of antibiotic wastewater. *Chem. Eng. J.* **2020**, *384*, 123279. [[CrossRef](#)]
83. Liu, M.; Zhang, D.; Han, J.; Liu, C.; Ding, Y.; Wang, Z.; Wang, A. Adsorption enhanced photocatalytic degradation sulfadiazine antibiotic using porous carbon nitride nanosheets with carbon vacancies. *Chem. Eng. J.* **2020**, *382*, 123017. [[CrossRef](#)]
84. Kumar, R.; Barakat, M.A.; Al-Mur, B.A.; Alseroury, F.A.; Eniola, J.O. Photocatalytic degradation of cefoxitin sodium antibiotic using novel BN/CdAl₂O₄ composite. *J. Clean. Prod.* **2020**, *246*, 119076. [[CrossRef](#)]
85. Musial, J.; Mlynarczyk, D.T.; Stanisz, B.J. Photocatalytic Degradation of Sulfamethoxazole Using TiO₂-Based Materials—Perspectives for the Development of a Sustainable Water Treatment Technology. *Sci. Total Environ.* **2023**, *856*, 159122. [[CrossRef](#)]
86. Sharma, V.K.; Yngard, R.A.; Lin, Y. Silver Nanoparticles: Green Synthesis and Their Antimicrobial Activities. *Adv. Colloid Interface Sci.* **2009**, *145*, 83–96. [[CrossRef](#)]
87. Durgalakshmi, D.; Rajendran, S.; Naushad, M. Current Role of Nanomaterials in Environmental Remediation. In *Advanced Nanostructured Materials for Environmental Remediation. Environmental Chemistry for a Sustainable World*; Naushad, M., Rajendran, S., Gracia, F., Eds.; Springer: Cham, Switzerland, 2019; Volume 25. [[CrossRef](#)]
88. Singh, T.; Jayaprakash, A.; Alsuwaidi, M.; Madhavan, A.A. Green Synthesized Gold Nanoparticles with Enhanced Photocatalytic Activity. *Mater. Today Proc.* **2021**, *42*, 1166–1169. [[CrossRef](#)]

89. Raza, W.; Haque, M.M.; Muneer, M.; Fleisch, M.; Hakki, A.; Bahnemann, D. Photocatalytic Degradation of Different Chromophoric Dyes in Aqueous Phase Using La and Mo Doped TiO₂ Hybrid Carbon Spheres. *J. Alloys Compd.* **2015**, *632*, 837–844. [[CrossRef](#)]
90. Rajkumar, K.; Muthukumar, M.; Mangalaraja, R.V. Electrochemical Degradation of C.I. Reactive Orange 107 Using Gadolinium (Gd³⁺), Neodymium (Nd³⁺) and Samarium (Sm³⁺) Doped Cerium Oxide Nanoparticles. *Int. J. Ind. Chem.* **2015**, *6*, 285–295. [[CrossRef](#)]
91. Chang, J.H.; Cheng, S.F. The Remediation Performance of a Specific Electrokinetics Integrated with Zero-Valent Metals for Perchloroethylene Contaminated Soils. *J. Hazard. Mater.* **2006**, *131*, 153–162. [[CrossRef](#)]
92. Xie, G.; Zhang, K.; Guo, B.; Liu, Q.; Fang, L.; Gong, J.R. Graphene-Based Materials for Hydrogen Generation from Light-Driven Water Splitting. *Adv. Mater.* **2013**, *25*, 3820–3839. [[CrossRef](#)] [[PubMed](#)]
93. Kudo, A.; Miseki, Y. Heterogeneous Photocatalyst Materials for Water Splitting. *Chem. Soc. Rev.* **2008**, *38*, 253–278. [[CrossRef](#)] [[PubMed](#)]
94. Wang, P.; Wang, J.; Huo, J.; Xu, W.; Wang, X.; Wang, G.; Wang, P.P.; Wang, J.Q.; Huo, J.T.; Xu, W.; et al. Fast Degradation of Azo Dye by Nanocrystallized Fe-Based Alloys. *Sci. China Phys. Mech. Astron.* **2017**, *60*, 076112. [[CrossRef](#)]
95. Tong, H.; Ouyang, S.; Bi, Y.; Umezawa, N.; Oshikiri, M.; Ye, J. Nano-Photocatalytic Materials: Possibilities and Challenges. *Adv. Mater.* **2012**, *24*, 229–251. [[CrossRef](#)]
96. Gaya, U.I.; Abdulllah, A.H. Heterogeneous Photocatalytic Degradation of Organic Contaminants over Titanium Dioxide: A Review of Fundamentals, Progress and Problems. *J. Photochem. Photobiol. C Photochem. Rev.* **2008**, *9*, 1–12. [[CrossRef](#)]
97. Fujishima, A.; Zhang, X.; Tryk, D.A. TiO₂ Photocatalysis and Related Surface Phenomena. *Surf. Sci. Rep.* **2008**, *63*, 515–582. [[CrossRef](#)]
98. Fujishima, A.; Honda, K. Electrochemical Photolysis of Water at a Semiconductor Electrode. *Nature* **1972**, *238*, 37–38. [[CrossRef](#)]
99. Xuan, J.; Xiao, W.J. Visible-Light Photoredox Catalysis. *Angew. Chem. Int. Ed.* **2012**, *51*, 6828–6838. [[CrossRef](#)]
100. Tu, W.; Zhou, Y.; Zou, Z. Photocatalytic Conversion of CO₂ into Renewable Hydrocarbon Fuels: State-of-the-Art Accomplishment, Challenges, and Prospects. *Adv. Mater.* **2014**, *26*, 4607–4626. [[CrossRef](#)]
101. Yang, G.; Yan, W.; Zhang, Q.; Shen, S.; Ding, S. One-Dimensional CdS/ZnO Core/Shell Nanofibers via Single-Spinneret Electrospinning: Tunable Morphology and Efficient Photocatalytic Hydrogen Production. *Nanoscale* **2013**, *5*, 12432–12439. [[CrossRef](#)]
102. Wetchakun, N.; Chaiwichain, S.; Inceesungvorn, B.; Pingmuang, K.; Phanichphant, S.; Minett, A.I.; Chen, J. BiVO₄/CeO₂ Nanocomposites with High Visible-Light-Induced Photocatalytic Activity. *ACS Appl. Mater. Interfaces* **2012**, *4*, 3718–3723. [[CrossRef](#)] [[PubMed](#)]
103. Hu, S.; Zhou, F.; Wang, L.; Zhang, J. Preparation of Cu₂O/CeO₂ Heterojunction Photocatalyst for the Degradation of Acid Orange 7 under Visible Light Irradiation. *Catal. Commun.* **2011**, *12*, 794–797. [[CrossRef](#)]
104. Li, J.; Guo, S.; Zhai, Y.; Wang, E. Nafion–Graphene Nanocomposite Film as Enhanced Sensing Platform for Ultrasensitive Determination of Cadmium. *Electrochem. Commun.* **2009**, *11*, 1085–1088. [[CrossRef](#)]
105. Li, C.; Chen, R.; Zhang, X.; Shu, S.; Xiong, J.; Zheng, Y.; Dong, W. Electrospinning of CeO₂–ZnO Composite Nanofibers and Their Photocatalytic Property. *Mater. Lett.* **2011**, *65*, 1327–1330. [[CrossRef](#)]
106. Li, K.; Lu, X.; Zhang, Y.; Liu, K.; Huang, Y.; Liu, H. Bi₃TaO₇/Ti₃C₂ Heterojunctions for Enhanced Photocatalytic Removal of Water-Borne Contaminants. *Environ. Res.* **2020**, *185*, 109409. [[CrossRef](#)]
107. Huang, Y.; Fan, W.; Long, B.; Li, H.; Zhao, F.; Liu, Z.; Tong, Y.; Ji, H. Visible light Bi₂S₃/Bi₂O₃/Bi₂O₂CO₃ photocatalyst for effective degradation of organic pollutions. *Appl. Catal. B Environ.* **2016**, *185*, 68–76. [[CrossRef](#)]
108. Navalon, S.; Alvaro, M.; Garcia, H. Heterogeneous Fenton Catalysts Based on Clays, Silicas and Zeolites. *Appl. Catal. B Environ.* **2010**, *99*, 1–26. [[CrossRef](#)]
109. Baldrian, P. Wood-Inhabiting Ligninolytic Basidiomycetes in Soils: Ecology and Constraints for Applicability in Bioremediation. *Fungal Ecol.* **2008**, *1*, 4–12. [[CrossRef](#)]
110. Corma, A.; García, H. Lewis Acids: From Conventional Homogeneous to Green Homogeneous and Heterogeneous Catalysis. *Chem. Rev.* **2003**, *103*, 4307–4365. [[CrossRef](#)]
111. Pera-Titus, M.; García-Molina, V.; Baños, M.A.; Giménez, J.; Esplugas, S. Degradation of Chlorophenols by Means of Advanced Oxidation Processes: A General Review. *Appl. Catal. B Environ.* **2004**, *47*, 219–256. [[CrossRef](#)]
112. Astruc, D.; Lu, F.; Aranzas, J.R. Nanoparticles as Recyclable Catalysts: The Frontier between Homogeneous and Heterogeneous Catalysis. *Angew. Chem. Int. Ed.* **2005**, *44*, 7852–7872. [[CrossRef](#)] [[PubMed](#)]
113. Nazim, M.; Khan, A.A.P.; Asiri, A.M.; Kim, J.H. Exploring Rapid Photocatalytic Degradation of Organic Pollutants with Porous CuO Nanosheets: Synthesis, Dye Removal, and Kinetic Studies at Room Temperature. *ACS Omega* **2021**, *6*, 2601–2612. [[CrossRef](#)] [[PubMed](#)]
114. Gupta, N.K.; Ghaffari, Y.; Kim, S.; Bae, J.; Kim, K.S.; Saifuddin, M. Photocatalytic Degradation of Organic Pollutants over MFe₂O₄ (M=Co, Ni, Cu, Zn) Nanoparticles at Neutral PH. *Sci. Rep.* **2020**, *10*, 4942. [[CrossRef](#)] [[PubMed](#)]
115. Kirankumar, V.S.; Sumathi, S. Structural, Optical, Magnetic and Photocatalytic Properties of Bismuth Doped Copper Aluminate Nanoparticles. *Mater. Chem. Phys.* **2017**, *197*, 17–26. [[CrossRef](#)]
116. Kumar, S.; Sahare, P.D. Photocatalytic activity of bismuth vanadate for the degradation of organic compounds. *Nano* **2013**, *8*, 1350007. [[CrossRef](#)]

117. Saygi, B.; Tekin, D. Photocatalytic Degradation Kinetics of Reactive Black 5 (RB5) Dyestuff on TiO₂ Modified by Pretreatment with Ultrasound Energy. *React. Kinet. Mech. Catal.* **2013**, *110*, 251–258. [[CrossRef](#)]
118. Ateş, S.; Baran, E.; Yazıcı, B. Fabrication of Al₂O₃ Nanopores/SnO₂ and Its Application in Photocatalytic Degradation under UV Irradiation. *Mater. Chem. Phys.* **2018**, *214*, 17–27. [[CrossRef](#)]
119. Alafif, Z.O.; Anjum, M.; Ansari, M.O.; Kumar, R.; Rashid, J.; Madkour, M.; Barakat, M.A. Synthesis and Characterization of S-Doped-RGO/ZnS Nanocomposite for the Photocatalytic Degradation of 2-Chlorophenol and Disinfection of Real Dairy Wastewater. *J. Photochem. Photobiol. A Chem.* **2019**, *377*, 190–197. [[CrossRef](#)]
120. Rao, M.P.C.; Kulandaivelu, K.; Ponnusamy, V.K.; Wu, J.J.; Sambandam, A. Surfactant-Assisted Synthesis of Copper Oxide Nanorods for the Enhanced Photocatalytic Degradation of Reactive Black 5 Dye in Wastewater. *Environ. Sci. Pollut. Res.* **2020**, *27*, 17438–17445. [[CrossRef](#)]
121. Akram, N.; Guo, J.; Ma, W.; Guo, Y.; Hassan, A.; Wang, J. Synergistic Catalysis of Co(OH)₂/CuO for the Degradation of Organic Pollutant Under Visible Light Irradiation. *Sci. Rep.* **2020**, *10*, 1939. [[CrossRef](#)]
122. Deng, X.; Wang, C.; Yang, H.; Shao, M.; Zhang, S.; Wang, X.; Ding, M.; Huang, J.; Xu, X. One-Pot Hydrothermal Synthesis of CdS Decorated CuS Microflower-like Structures for Enhanced Photocatalytic Properties. *Sci. Rep.* **2017**, *7*, 3877. [[CrossRef](#)] [[PubMed](#)]
123. Dutta, S.; Gupta, B.; Srivastava, S.K.; Gupta, A.K. Recent Advances on the Removal of Dyes from Wastewater Using Various Adsorbents: A Critical Review. *Mater. Adv.* **2021**, *2*, 4497–4531. [[CrossRef](#)]
124. Nadeem Baig; Irshad Kammakam; Wail Falath Nanomaterials: A Review of Synthesis Methods, Properties, Recent Progress, and Challenges. *Mater. Adv.* **2021**, *2*, 1821–1871. [[CrossRef](#)]
125. Thirunavukkarasu, A.; Muthukumar, K.; Nithya, R. Adsorption of Acid Yellow 36 onto Green Nanoceria and Amine Functionalized Green Nanoceria: Comparative Studies on Kinetics, Isotherm, Thermodynamics, and Diffusion Analysis. *J. Taiwan Inst. Chem. Eng.* **2018**, *93*, 211–225. [[CrossRef](#)]
126. Rajarathinam, N.; Arunachalam, T.; Raja, S.; Selvasembian, R. Fenalan Yellow G Adsorption Using Surface-Functionalized Green Nanoceria: An Insight into Mechanism and Statistical Modelling. *Environ. Res.* **2020**, *181*, 108920. [[CrossRef](#)]
127. Mirjavadi, E.S.; Tehrani, R.M.A.; Khadir, A. Effective Adsorption of Zinc on Magnetic Nanocomposite of Fe₃O₄/Zeolite/Cellulose Nanofibers: Kinetic, Equilibrium, and Thermodynamic Study. *Environ. Sci. Pollut. Res.* **2019**, *26*, 33478–33493. [[CrossRef](#)]
128. Rangabhashiyam, S.; Suganya, E.; Lity, A.V.; Selvaraju, N. Equilibrium and Kinetics Studies of Hexavalent Chromium Biosorption on a Novel Green *Macroalgae enteromorpha* sp. *Res. Chem. Intermed.* **2015**, *42*, 1275–1294. [[CrossRef](#)]
129. Zach-Maor, A.; Semiat, R.; Shemer, H. Removal of Heavy Metals by Immobilized Magnetite Nano-Particles. *New Pub Balaban* **2012**, *31*, 64–70. [[CrossRef](#)]
130. Kumar, K.Y.; Muralidhara, H.B.; Nayaka, Y.A.; Balasubramanyam, J.; Hanumanthappa, H. Low-Cost Synthesis of Metal Oxide Nanoparticles and Their Application in Adsorption of Commercial Dye and Heavy Metal Ion in Aqueous Solution. *Powder Technol.* **2013**, *246*, 125–136. [[CrossRef](#)]
131. Arikal, D.; Kallingal, A. Photocatalytic Degradation of Azo and Anthraquinone Dye Using TiO₂/MgO Nanocomposite Immobilized Chitosan Hydrogels. *Environ. Technol.* **2021**, *42*, 2278–2291. [[CrossRef](#)]
132. Yang, X.; Liu, Y.; Li, J.; Zhang, Y. Effects of Calcination Temperature on Morphology and Structure of CeO₂ Nanofibers and Their Photocatalytic Activity. *Mater. Lett.* **2019**, *241*, 76–79. [[CrossRef](#)]
133. Hitkari, G.; Chowdhary, P.; Kumar, V.; Singh, S.; Motghare, A. Potential of Copper-Zinc Oxide Nanocomposite for Photocatalytic Degradation of Congo Red Dye. *Clean. Chem. Eng.* **2022**, *1*, 100003. [[CrossRef](#)]
134. Zhao, P.; Zhao, Y.; Guo, Y.; Guo, R.; Tian, Y.; Zhao, W. Preparation of CuO/γAl₂O₃ Catalyst for Degradation of Azo Dyes (Reactive Brilliant Red X-3B): An Optimization Study. *J. Clean. Prod.* **2021**, *328*, 129624. [[CrossRef](#)]
135. Rizvi, M.; Tiwari, N.; Mishra, A.; Gupta, R. Kinetic and Computational Study of Degradation of Two Azo Dyes, Metanil Yellow and Orange II, by Iron Oxide Nanoparticles Synthesized Using *Hylocereus Undatus*. *ACS Omega* **2022**, *7*, 31667–31681. [[CrossRef](#)]
136. Ait Himi, M.; El Ghachtouli, S.; Amarray, A.; Zaroual, Z.; Bonnaillie, P.; Azzi, M. Nanostructured Manganese Oxide as an Efficient Eco-Friendly Catalyst for Removing Azo Dye Calcon from Water. *Mater. Sci.* **2020**, *37*, 3905–3912. [[CrossRef](#)]
137. Ullah, A.; Rahman, L.; Hussain, S.Z.; Abbas, W.; Tawab, A.; Jilani, A.; Bajwa, S.Z.; Khan, W.S.; Riaz, R.; Hussain, I.; et al. Mechanistic Insight of Dye Degradation Using TiO₂ Anchored α-MnO₂ Nanorods as Promising Sunlight Driven Photocatalyst. *Mater. Sci. Eng. B* **2021**, *271*, 115257. [[CrossRef](#)]
138. Salari, H.; Yaghmaei, H. Z-Scheme 3D Bi₂WO₆/MnO₂ Heterojunction for Increased Photoinduced Charge Separation and Enhanced Photocatalytic Activity. *Appl. Surf. Sci.* **2020**, *532*, 147413. [[CrossRef](#)]
139. Madima, N.; Mishra, S.B.; Inamuddin, I.; Mishra, A.K. Carbon-Based Nanomaterials for Remediation of Organic and Inorganic Pollutants from Wastewater. A Review. *Environ. Chem. Lett.* **2020**, *18*, 1169–1191. [[CrossRef](#)]
140. Mashkoo, F.; Nasar, A. Inamuddin Carbon Nanotube-Based Adsorbents for the Removal of Dyes from Waters: A Review. *Environ. Chem. Lett.* **2020**, *18*, 605–629. [[CrossRef](#)]
141. Visakh, P.M. Introduction for Nanomaterials and Nanocomposites: State of Art, New Challenges, and Opportunities. In *Nanomaterials and Nanocomposites: Zero to Three-Dimensional Materials and Their Composites*; Wiley: Hoboken, NJ, USA, 2016; pp. 1–20. [[CrossRef](#)]
142. Ren, X.; Chen, C.; Nagatsu, M.; Wang, X. Carbon Nanotubes as Adsorbents in Environmental Pollution Management: A Review. *Chem. Eng. J.* **2011**, *170*, 395–410. [[CrossRef](#)]

143. Yang, K.; Xing, B. Adsorption of Organic Compounds by Carbon Nanomaterials in Aqueous Phase: Polanyi Theory and Its Application. *Chem. Rev.* **2010**, *110*, 5989–6008. [[CrossRef](#)] [[PubMed](#)]
144. Chen, W.; Duan, L.; Zhu, D. Adsorption of Polar and Nonpolar Organic Chemicals to Carbon Nanotubes. *Environ. Sci. Technol.* **2007**, *41*, 8295–8300. [[CrossRef](#)] [[PubMed](#)]
145. Yang, K.; Wu, W.; Jing, Q.; Zhu, L. Aqueous Adsorption of Aniline, Phenol, and Their Substitutes by Multi-Walled Carbon Nanotubes. *Environ. Sci. Technol.* **2008**, *42*, 7931–7936. [[CrossRef](#)] [[PubMed](#)]
146. Mengesha, D.N.; Kim, H. Electronic Structure Modulation of Multi-Walled Carbon Nanotubes Using Azo Dye for Inducing Non-Radical Reaction: Effect of Graphitic Nitrogen and Structural Defect. *Chemosphere* **2022**, *307*, 136023. [[CrossRef](#)] [[PubMed](#)]
147. Luan, N.H.; Yang, Y.T.; Chang, C.F. Electrochemical Degradation of Methylene Blue Accompanied with the Reduction of CO₂ by Using Carbon Nanotubes Grown on Carbon Fiber Electrodes. *Sustain. Environ. Res.* **2022**, *32*, 13. [[CrossRef](#)]
148. Khan, J.; Ilyas, S.; Akram, B.; Ahmad, K.; Hafeez, M.; Siddiq, M.; Ashraf, M.A. Zn/NiO Coated Multi-Walled Carbon Nanotubes for Textile Dyes Degradation. *Arab. J. Chem.* **2018**, *11*, 880–896. [[CrossRef](#)]
149. De Luca, P.; Nagy, J.B. Treatment of Water Contaminated with Reactive Black-5 Dye by Carbon Nanotubes. *Materials* **2020**, *13*, 5508. [[CrossRef](#)]
150. Hemraj-Benny, T.; Pimentel, L.; Emeran, G. Formation of Single-Walled Carbon Nanotube-Ruthenium Nanoparticles in Ethanol upon Microwave Radiation. *Inorg. Chem. Commun.* **2020**, *112*, 107707. [[CrossRef](#)]
151. Naghizadeh, A.; Karimi, A.; Derakhshani, E.; Esform, A. Single-Walled Carbon Nanotubes (SWCNTs) as an Efficient Adsorbent for Removal of Reactive Dyes from Water Solution: Equilibrium, Kinetic, and Thermodynamic. *Environ. Qual. Manag.* **2022**, *31*, 133–140. [[CrossRef](#)]
152. Agarwal, M.; Kumari, P.; Dubey, S.; Gupta, R.; Dohare, R.K. Adsorption Behavior of Azo Dyes on Carbon Nanotubes Grown on Alumina: Process Optimization, Kinetics, and Equilibrium Study. *J. Environ. Eng.* **2018**, *145*, 04018134. [[CrossRef](#)]
153. Liu, L.; Liu, S.; Zhang, Q.; Li, C.; Bao, C.; Liu, X.; Xiao, P. Adsorption of Au(III), Pd(II), and Pt(IV) from Aqueous Solution onto Graphene Oxide. *J. Chem. Eng. Data* **2013**, *58*, 209–216. [[CrossRef](#)]
154. Machida, M.; Mochimaru, T.; Tatsumoto, H. Lead(II) Adsorption onto the Graphene Layer of Carbonaceous Materials in Aqueous Solution. *Carbon* **2006**, *44*, 2681–2688. [[CrossRef](#)]
155. Yang, S.T.; Chang, Y.; Wang, H.; Liu, G.; Chen, S.; Wang, Y.; Liu, Y.; Cao, A. Folding/Aggregation of Graphene Oxide and Its Application in Cu²⁺ Removal. *J. Colloid Interface Sci.* **2010**, *351*, 122–127. [[CrossRef](#)] [[PubMed](#)]
156. Wang, H.; Yuan, X.; Wu, Y.; Huang, H.; Zeng, G.; Liu, Y.; Wang, X.; Lin, N.; Qi, Y. Adsorption Characteristics and Behaviors of Graphene Oxide for Zn(II) Removal from Aqueous Solution. *Appl. Surf. Sci.* **2013**, *279*, 432–440. [[CrossRef](#)]
157. Bian, Y.; Bian, Z.Y.; Zhang, J.X.; Ding, A.Z.; Liu, S.L.; Wang, H. Effect of the Oxygen-Containing Functional Group of Graphene Oxide on the Aqueous Cadmium Ions Removal. *Appl. Surf. Sci.* **2015**, *329*, 269–275. [[CrossRef](#)]
158. Gao, W.; Majumder, M.; Alemany, L.B.; Narayanan, T.N.; Ibarra, M.A.; Pradhan, B.K.; Ajayan, P.M. Engineered Graphite Oxide Materials for Application in Water Purification. *ACS Appl. Mater. Interfaces* **2011**, *3*, 1821–1826. [[CrossRef](#)]
159. Lingamdinne, L.P.; Koduru, J.R.; Choi, Y.-L.; Chang, Y.-Y.; Yang, J.-K. Studies on Removal of Pb(II) and Cr(III) Using Graphene Oxide Based Inverse Spinel Nickel Ferrite Nano-Composite as Sorbent. *Hydrometallurgy* **2016**, *165*, 64–72. [[CrossRef](#)]
160. Upadhyay, R.K.; Soin, N.; Roy, S.S. Role of Graphene/Metal Oxide Composites as Photocatalysts, Adsorbents and Disinfectants in Water Treatment: A Review. *RSC Adv.* **2014**, *4*, 3823–3851. [[CrossRef](#)]
161. Jayanthi, S.; Krishnarao Eswar, N.; Singh, S.A.; Chatterjee, K.; Madras, G.; Sood, A.K. Macroporous Three-Dimensional Graphene Oxide Foams for Dye Adsorption and Antibacterial Applications. *RSC Adv.* **2016**, *6*, 1231–1242. [[CrossRef](#)]
162. Konicki, W.; Aleksandrak, M.; Moszyński, D.; Mijowska, E. Adsorption of Anionic Azo-Dyes from Aqueous Solutions onto Graphene Oxide: Equilibrium, Kinetic and Thermodynamic Studies. *J. Colloid Interface Sci.* **2017**, *496*, 188–200. [[CrossRef](#)]
163. Fan, L.; Luo, C.; Li, X.; Lu, F.; Qiu, H.; Sun, M. Fabrication of Novel Magnetic Chitosan Grafted with Graphene Oxide to Enhance Adsorption Properties for Methyl Blue. *J. Hazard. Mater.* **2012**, *215–216*, 272–279. [[CrossRef](#)] [[PubMed](#)]
164. Saroyan, H.; Kyzas, G.Z.; Deliyanni, E.A. Effective Dye Degradation by Graphene Oxide Supported Manganese Oxide. *Processes* **2019**, *7*, 40. [[CrossRef](#)]
165. Idoia Martín-de-Lucía, C.; Campos-Mañas, M.; Agüera, A.; Rodea-Palomares, I.; Pulido-Reyes, G.; Leganés, F.; Fernández-Piñas, F. Roberto Rosal Reverse Trojan-Horse Effect Decreased Wastewater Toxicity in the Presence of Inorganic Nanoparticles. *Environ. Sci. Nano* **2017**, *4*, 1273–1282. [[CrossRef](#)]
166. Mahmoodi, N.M.; Maghsoodi, A. Kinetics and Isotherm of Cationic Dye Removal from Multicomponent System Using the Synthesized Silica Nanoparticle. *Desalination Water Treat.* **2014**, *54*, 562–571. [[CrossRef](#)]
167. Da'na, E. Nano-Silica Modified with Diamine for Capturing Azo Dye from Aqueous Solutions. *Molecule* **2022**, *27*, 3366. [[CrossRef](#)]
168. Vinoda, B.M.; Vinuth, M. Photocatalytic Degradation of Toxic Methyl Red Dye Using Silica Nanoparticles Synthesized from Rice Husk Ash. *J. Environ. Anal. Toxicol.* **2015**, *5*, 1000336. [[CrossRef](#)]
169. Chen, J.; Sheng, Y.; Song, Y.; Chang, M.; Zhang, X.; Cui, L.; Meng, D.; Zhu, H.; Shi, Z.; Zou, H. Multimorphology Mesoporous Silica Nanoparticles for Dye Adsorption and Multicolor Luminescence Applications. *ACS Sustain. Chem. Eng.* **2018**, *6*, 3533–3545. [[CrossRef](#)]
170. Alswieleh, A.M. Efficient Removal of Dyes from Aqueous Solution by Adsorption on L-Arginine-Modified Mesoporous Silica Nanoparticles. *Processes* **2022**, *10*, 1079. [[CrossRef](#)]

171. Sahoo, A.; Patra, S. A Combined Process for the Degradation of Azo-Dyes and Efficient Removal of Aromatic Amines Using Porous Silicon Supported Porous Ruthenium Nanocatalyst. *ACS Appl. Nano Mater.* **2018**, *1*, 5169–5178. [[CrossRef](#)]
172. Ekka, B.; Sahu, M.K.; Patel, R.K.; Dash, P. Titania Coated Silica Nanocomposite Prepared via Encapsulation Method for the Degradation of Safranin-O Dye from Aqueous Solution: Optimization Using Statistical Design. *Water Resour. Ind.* **2019**, *22*, 100071. [[CrossRef](#)]
173. Jhaveri, J.H.; Murthy, Z.V.P. A Comprehensive Review on Anti-Fouling Nanocomposite Membranes for Pressure Driven Membrane Separation Processes. *Desalination* **2016**, *379*, 137–154. [[CrossRef](#)]
174. Reddy, A.S.; Kalla, S.; Murthy, Z.V.P. Nano-Particles Enhanced Hydrophobic Membranes: High-Performance Study for Dye Wastewater Treatment Using Membrane Distillation. *J. Water Process Eng.* **2022**, *46*, 102610. [[CrossRef](#)]
175. Yang, B.; Geng, P.; Chen, G. One-Dimensional Structured IrO₂ Nanorods Modified Membrane for Electrochemical Anti-Fouling in Filtration of Oily Wastewater. *Sep. Purif. Technol.* **2015**, *156*, 931–941. [[CrossRef](#)]
176. Pendergast, M.M.; Hoek, E.M.V. A Review of Water Treatment Membrane Nanotechnologies. *Energy Environ. Sci.* **2011**, *4*, 1946–1971. [[CrossRef](#)]
177. Forgacs, E.; Cserháti, T.; Oros, G. Removal of Synthetic Dyes from Wastewaters: A Review. *Environ. Int.* **2004**, *30*, 953–971. [[CrossRef](#)]
178. Singh, K.; Arora, S. Removal of Synthetic Textile Dyes from Wastewaters: A Critical Review on Present Treatment Technologies. *Crit. Rev. Environ. Sci. Technol.* **2011**, *41*, 807–878. [[CrossRef](#)]
179. Aliabadi, M.; Irani, M.; Ismaeili, J.; Piri, H.; Parnian, M.J. Electrospun Nanofiber Membrane of PEO/Chitosan for the Adsorption of Nickel, Cadmium, Lead and Copper Ions from Aqueous Solution. *Chem. Eng. J.* **2013**, *220*, 237–243. [[CrossRef](#)]
180. Deng, J.; Kang, X.; Chen, L.; Wang, Y.; Gu, Z.; Lu, Z. A Nanofiber Functionalized with Dithizone by Co-Electrospinning for Lead (II) Adsorption from Aqueous Media. *J. Hazard. Mater.* **2011**, *196*, 187–193. [[CrossRef](#)]
181. Wu, S.; Li, F.; Wang, H.; Fu, L.; Zhang, B.; Li, G. Effects of Poly (Vinyl Alcohol) (PVA) Content on Preparation of Novel Thiol-Functionalized Mesoporous PVA/SiO₂ Composite Nanofiber Membranes and Their Application for Adsorption of Heavy Metal Ions from Aqueous Solution. *Polymer* **2010**, *51*, 6203–6211. [[CrossRef](#)]
182. Asouhidou, D.D.; Triantafyllidis, K.S.; Lazaridis, N.K.; Matis, K.A. Adsorption of Remazol Red 3BS from Aqueous Solutions Using APTES- and Cyclodextrin-Modified HMS-Type Mesoporous Silicas. *Colloids Surfaces A Physicochem. Eng. Asp.* **2009**, *346*, 83–90. [[CrossRef](#)]
183. Akduman, C.; Akçakoca Kumbasar, E.P.; Morsunbul, S. Electrospun Nanofiber Membranes for Adsorption of Dye Molecules from Textile Wastewater. *IOP Conf. Ser. Mater. Sci. Eng.* **2017**, *254*, 102001. [[CrossRef](#)]
184. Long, Q.; Zhang, Z.; Qi, G.; Wang, Z.; Chen, Y.; Liu, Z.-Q. Fabrication of Chitosan Nanofiltration Membranes by the Film Casting Strategy for Effective Removal of Dyes/Salts in Textile Wastewater. *ACS Sustain. Chem. Eng.* **2020**, *8*, 2512–2522. [[CrossRef](#)]
185. Hassan, A.R.; Rozali, S.; Safari, N.H.M.; Besar, B.H. The Roles of Polyethersulfone and Polyethylene Glycol Additive on Nanofiltration of Dyes and Membrane Morphologies. *Environ. Eng. Res.* **2018**, *23*, 316–322. [[CrossRef](#)]
186. Gunawan, F.M.; Mangindaan, D.; Khoiruddin, K.; Wenten, I.G. Nanofiltration Membrane Cross-Linked by m-Phenylenediamine for Dye Removal from Textile Wastewater. *Polym. Adv. Technol.* **2019**, *30*, 360–367. [[CrossRef](#)]
187. Buscio, V.; García-Jiménez, M.; Vilaseca, M.; López-Grimau, V.; Crespi, M.; Gutiérrez-Bouzán, C. Reuse of Textile Dyeing Effluents Treated with Coupled Nanofiltration and Electrochemical Processes. *Materials* **2016**, *9*, 490. [[CrossRef](#)] [[PubMed](#)]
188. Askari, N.; Farhadian, M.; Razmjou, A.; Hashtroudi, H. Nanofiltration Performance in the Removal of Dye from Binary Mixtures Containing Anthraquinone Dyes. *Desalination Water Treat.* **2015**, *57*, 18194–18201. [[CrossRef](#)]
189. Zhang, M.; Field, R.W.; Zhang, K. Biogenic Silver Nanocomposite Polyethersulfone UF Membranes with Antifouling Properties. *J. Memb. Sci.* **2014**, *471*, 274–284. [[CrossRef](#)]